https://doi.org/10.5194/egusphere-2026-2165
Preprint. Discussion started: 10 June 2026

Assessment of methane emissions from European countries using satellite and surface observations

Shuai Sun[1,2,3], Yuzhong Zhang[2,3*], Wei Chen[1,2,3], Shaomin Pan[1,2,3], Dongchuan Pu[4], Xin Tong[5], Huilin Chen[5], Sander Houweling[6,7]

[1]College of Environmental and Resource Sciences, Zhejiang University, Hangzhou, Zhejiang 310058, China
[2]Key Laboratory of Coastal Environment and Resources of Zhejiang Province, School of Engineering, Westlake University, Hangzhou, Zhejiang 310030, China
[3]Institute of Advanced Technology, Westlake Institute for Advanced Study, Hangzhou, Zhejiang 310024, China
[4]Research Institute for Smart Cities, School of Architecture and Urban Planning, Shenzhen University, Shenzhen, PR China
[5]Joint International Research Laboratory of Atmospheric and Earth System Sciences, School of Atmospheric Sciences, Nanjing University, 210023, Nanjing, China
[6]Department of Earth Sciences, Vrije Universiteit, Amsterdam, the Netherlands
[7]SRON, Netherlands Institute for Space Research, Leiden, the Netherlands

Correspondence to: Yuzhong Zhang (zhangyuzhong@westlake.edu.cn)

Abstract: Europe is a global leader in mitigating methane emissions through comprehensive policies, including the EU Methane Strategy and commitments under the Global Methane Pledge. National bottom-up inventories are widely regarded as high quality; however, atmospheric observations remain essential for independent verification and tracking emission reductions. Here, we present a multi-year (2019–2023) top-down assessment of European methane emissions using a Bayesian inversion of satellite observations from TROPOMI and surface measurements from ICOS. Analysis of observational constraints shows that surface measurements provide the dominant information, while satellite observations offer complementary coverage in regions not covered by the surface network. The inversion estimates total European methane emissions at 24.7 Tg yr^{-1}, including 22.1 Tg yr^{-1} from anthropogenic sources, which is 1.0 Tg yr^{-1} higher than the prior inventory. The upward revision is mainly attributed to livestock and waste emissions in central and western Europe, partly offset by lower fossil fuel emissions in the North Sea. National emissions for the Netherlands, Germany, and Italy are 27–62% higher than reported to the UNFCCC. The inversion also reveals an overall decline in anthropogenic emissions (–0.27 Tg yr^{-2}). While consistent in magnitude with the prior estimate, the inversion shows a distinct spatial pattern: increases in livestock and waste emissions in western Europe contrast with decreases in fossil fuel production regions such as the North Sea and Poland. These findings highlight the value of atmospheric observations for evaluating methane inventories and informing climate policy.

Key words: Europe, methane emissions, inversion, satellite

https://doi.org/10.5194/egusphere-2026-2165
Preprint. Discussion started: 10 June 2026

1 Introduction

Methane (CH_4) is a strong greenhouse gas with a global warming potential ~30 times that of CO_2 over 100 years. Increases in atmospheric methane concentrations since industrialization result in 0.54 W m^{-2} effective radiative forcing, making it the second most important anthropogenic greenhouse gas after carbon dioxide (CO_2) (IPCC, 2021). Methane is emitted from various anthropogenic sources including fossil fuel production and use (oil, gas, and coal), agriculture (livestock and rice cultivation), and waste management (landfills and wastewater) (Fu et al., 2024; Saunois et al., 2020). Natural sources, dominated by wetlands, are also main contributor to the global methane budget (Kirschke et al., 2013; Zhang et al., 2023). Rapid reduction of methane emissions is a critical strategy for mitigating near-term warming, creating a crucial window for implementing long-term deep decarbonization (Nisbet et al., 2020; Szopa et al., 2021).

Europe has positioned itself as a global leader in methane mitigation. The methane mitigation policy of the European Union (EU) is anchored in the EU Methane Strategy (2020) and its commitment to the Global Methane Pledge, which aims for a 30% reduction in global methane emissions by 2030 relative to 2020 levels. The EU approved the landmark Methane Regulation (EU) 2024/1787 in May 2024, which includes mandatory source-level measurement, reporting, and verification, frequent leak detection and repair (LDAR), a ban on routine venting and flaring mandatory leak detection, flaring bans, and import standards on methane intensity (European Union, 2024). To address the agriculture and waste sectors, the revised Industrial and Livestock Rearing Emissions Directive (IED 2.0) imposes binding emission controls on the largest livestock farms, while the Landfill Directive mandates a reduction of municipal waste in landfills to 10% by 2035.

Accurate quantification of methane emissions is critical for implementing policies and verifying progress. Under the Paris Agreement's enhanced transparency framework, European countries submit national greenhouse gas inventories to the UNFCCC on a regular basis. Many countries employ high-tier, methodologically advanced accounting practices in compiling these inventories, reflecting Europe's leading role in the development of reporting systems (EEA, 2024). However, persistent uncertainties from unaccounted emission sources or methodological biases necessitate independent verification. Top-down approaches, which infer emissions from atmospheric observations using inverse modeling, offer a powerful, objective

https://doi.org/10.5194/egusphere-2026-2165
Preprint. Discussion started: 10 June 2026

complement to traditional bottom-up inventories (Houweling et al., 2017; Jacob et al., 2022; Wang et al., 2025). Pioneering efforts, such as those by the United Kingdom, have been made to incorporate atmospheric verification into official national greenhouse gas inventory reporting (Manning et al., 2011).

The top-down approach relies on atmospheric observations. Satellite observations from GOSAT and TROPOMI have been widely used to estimate emissions at regional and national scales across diverse geographies (e.g., Shen et al., 2022; Zhang et al., 2020; Hancock et al., 2024; Chen et al., 2023; Chen et al., 2022; Liang et al., 2022, 2024). In Europe, the high-quality Integrated Carbon Observation System, mainly deployed in Western Europe, provides another critical data stream (Pison et al., 2018). Recent studies applying ICOS data have successfully quantified emissions in the Benelux countries (Bruch et al., 2025; Steiner et al., 2024). The integration of surface and satellite data have demonstrated complementary capabilities in constraining global (Lu et al., 2023a) and regional (Lu et al., 2023b; Zhang et al., 2022) methane emissions.

In this study, we conduct a multi-year (2019–2023) inversion analysis of methane emissions over Europe, leveraging high-resolution TROPOMI satellite data and hourly high-quality ICOS measurements. By comparing posterior emissions with both prior inventories and national reports to the UNFCCC, we assess the consistency of emission estimates across sources, regions, and years. This integrated top-down analysis aims to provide improved constraints on methane emissions in Europe, identify discrepancies with bottom-up inventories, and inform future policy and mitigation efforts under the Paris Agreement and the Global Methane Pledge.

2 Data and methods

2.1 Satellite observations

We use column-averaged dry-air methane mole fractions (XCH4) from the blended GOSAT+TROPOMI satellite product (referred to as TROPOMI observations hereafter), which employs CO_2 proxy GOSAT methane retrievals as a reference to correct the retrieval biases of original TROPOMI data (Balasus et al., 2023). We use retrievals over land from 2019 to 2023.

https://doi.org/10.5194/egusphere-2026-2165
Preprint. Discussion started: 10 June 2026

We exclude observations poleward of 55° owing to surface snow cover, unfavorable illumination, and possible stratospheric model biases (Hasekamp et al., 2021; Turner et al., 2015b; Zhang et al., 2025). The TROPOMI observations have a spatial resolution of 7 km × 5.5 km at nadir (previously 7 km × 7 km before August 2019) and a local overpass time of approximately 13:30 (Hu et al., 2016; Veefkind et al., 2012). XCH_4 is retrieved from measurements at the SWIR (2.3 μm) band, in combination with the NIR (757–774 nm) band.

Figure 1 shows the spatial distribution of 2019 annual average XCH4 concentrations and the number of observations across the study domain. On average, there are ~7.5×10^6 TROPOMI observations annually, with considerable spatial variability in observation density (Figure 1). For instance, in Western Europe, observation coverage is denser over Spain, Portugal, and France compared to neighboring Germany, Belgium, the Netherlands, and the United Kingdom. Satellite observations are sparse in in Northern Europe but moderate in Eastern Europe. This uneven spatial coverage influences the satellite's capacity to constrain methane emissions across different regions.

2.2 Surface observations

We also use ground-based methane observations from the Integrated Carbon Observation System (ICOS) network across Europe (https://www.icos-cp.eu/data-products/atmosphere-release; ICOS RI et al., 2025). We use hourly dry-air methane mole fraction observations from 31 ICOS atmospheric stations, flagged as flagged as valid after manual quality assurance (Flag = 'O'), during 2019–2023. We then compute daily daytime averages using data between 10:00 and 16:00 local time, which generally represent well-mixed boundary layer conditions.

Figure 2 shows the spatial distribution of the ICOS stations used in our analysis, alongside their 2023 mean methane concentrations. The surface sites are predominantly clustered in Western Europe centering Germany, the Netherlands and northern France (Figure 2). Additional sites are located in the UK and Northern Europe (Figure 2). These regions correspond to areas with sparse satellite data coverage (Figure 1), underscoring the strong complementarity between satellite and surface

https://doi.org/10.5194/egusphere-2026-2165
Preprint. Discussion started: 10 June 2026

observations for constraining methane emissions. Furthermore, the surface measurements reveal elevated methane concentrations in the Netherlands, northern Italy, and northwestern Germany (Figure 2), generally consistent with the hotspots of elevated XCH4 in satellite observations (Figure 1).

2.3 Prior emissions

Figure 3 shows the spatial distribution of prior emissions by sector in the inversion domain. Table S1 tabulates national totals and their sectoral breakdown. Prior anthropogenic emissions (including agriculture, fossil fuel, and waste) are taken from the Emissions Database for Global Atmospheric Research (EDGAR) v8 global emission inventory (Crippa et al., 2023). Prior natural emissions are compiled from multiple datasets: wetland emissions from the ensemble mean of WetCHARTs version 1.0 (Bloom et al., 2017), biomass burning emissions from the Quick Fire Emissions Dataset version 2 (QFED2), termite emissions from Fung et al. (1991), and geological emissions from Maasakkers et al. (2019).

These prior emission inventories yield a total methane emission of 25.2 Tg a^{-1} for the study domain, which is mainly from anthropogenic sources (22.0 Tg a^{-1}). The largest anthropogenic sector in Europe is livestock, distributed primarily in France, Germany, the Netherlands, and the UK. By contrast, rice cultivation is a minor agricultural source, mainly located in northern Italy. Oil and natural gas production are concentrated in the North Sea, while coal production in eastern Europe such as Poland. The waste sector, including wastewater and landfills, are typically associated with population-dense urban centers. Natural sources are dominated by northern high-latitude wetlands. The prior emission inventories indicate a steady decline in anthropogenic methane emissions from the European countries by 0.2 Tg a^{-2} (0.9% a^{-1}). The decrease is mainly driven by the waste sector in western Europe, the oil & gas sector in the North Sea, and the coal sector in Ukraine.

https://doi.org/10.5194/egusphere-2026-2165
Preprint. Discussion started: 10 June 2026

2.4 Forward model simulations

We employ the nested version of the GEOS-Chem 12.9.3 chemical transport model (https://zenodo.org/records/3974569) as the forward model for the inversion, which relates atmospheric concentrations to surface emissions. The simulation has a horizontal resolution of 0.5° × 0.625° over the European domain (30–70°N, -30–50°E) with 47 vertical layers, and is driven by MERRA-2 reanalysis meteorology from the NASA Global Modeling and Assimilation Office (GMAO) (Gelaro et al., 2017). The atmospheric oxidation of methane is simulated using archived monthly OH, Cl, and stratospheric loss fields (Wecht et al., 2014).

The initial and 3-h dynamic boundary conditions for the regional simulation are derived from a 4° × 5° global simulation, after applying a correction for systematic biases. These biases are estimated and corrected using satellite and surface observations from background grid cells near the western and northern boundaries, which are the primary inflow pathways into the domain (Figure S4). This correction substantially improves model performance against independent IAGOS-CARIBIC aircraft observations in the European free troposphere, reducing the mean bias from 14.1 ppb to 2.9 ppb (Figure 4). Free tropospheric methane concentrations are largely governed by boundary conditions rather than local surface emissions, making these aircraft data suitable for evaluating boundary conditions. This argument is further supported by the minimal change in simulated free tropospheric methane concentrations between the prior and posterior simulations (Figure 4).

To compare with satellite or surface observations, we sample methane fields simulated by GEOS-Chem at the location and time of observations. For surface data, we compute daily daytime averages (10:00–16:00 local time) as applied to the hourly in situ measurements. For satellite data, we compute column-averaged methane mole fractions by accounting the instrument's vertical sensitivity and the prior methane vertical profile.

https://doi.org/10.5194/egusphere-2026-2165
Preprint. Discussion started: 10 June 2026

2.5 Inversion procedure

The inversion optimizes a state vector x consisting of annual methane emissions from 824 spatial clusters across the study domain (819 clusters for land and 5 clusters for the North Sea, shown in Figure S1). We first assign the number of clusters to each country by accounting for the country's areas and prior methane emissions, and then generate spatial clusters using the Gaussian Mixture Model (GMM) (Turner and Jacob, 2015a) for each country.

We estimate the optimal solution of the state vector $\boldsymbol{x}$ by minimizing a Bayesian cost function that incorporates both prior knowledge and observational constraints (Brasseur and Jacob, 2017):

$$\boldsymbol{J(x)} = (\boldsymbol{x} - \boldsymbol{x}_a)^{\mathrm{T}}\mathbf{S}_{\boldsymbol{a}}^{-1}(\boldsymbol{x} - \boldsymbol{x}_a) + (\boldsymbol{y} - \boldsymbol{F(x)})^{\mathrm{T}}\mathbf{S}_{\boldsymbol{O}}^{-1}(\boldsymbol{y} - \boldsymbol{F(x)}) \quad (1)$$

where $\boldsymbol{y}$ is the observation vector that contains both satellite and surface observations, $\boldsymbol{x_a}$ denotes the prior estimate for $\boldsymbol{x}$, $\mathbf{S_a}$ is the prior error covariance matrix, $\mathbf{S_0}$ is the observing system error covariance matrix, and $\boldsymbol{F(x)}$ represents the forward simulation by GEOS-Chem. We treat $\mathbf{S_a}$ as a diagonal matrix with a 50% relative uncertainty assigned to each emission flux. $\mathbf{S_0}$ is also constructed as a diagonal matrix using the residual error method. We account for the effects of error covariance on observation power, following the methodologies of Zhang et al. (2022) and Liang et al. (2023); detailed calculations are provided in the Supplementary Material. Additionally, we perform sensitivity inversions in which the observation vector ($\boldsymbol{y}$) contains either satellite data alone or surface data alone. This allows us to examine the consistency between the two platforms and quantify the observational constraints provided by each.

Minimizing $\boldsymbol{J(x)}$ yields the analytic solutions for the optimal estimate,

$$\hat{\boldsymbol{x}} = \boldsymbol{x_a} + (\mathbf{K}^{\mathrm{T}}\mathbf{S}_{\mathbf{0}}^{-1}\mathbf{K} + \mathbf{S}_{\mathbf{a}}^{-1})^{-1}\mathbf{K}^{\mathrm{T}}\mathbf{S}_{\mathbf{0}}^{-1}(\boldsymbol{y} - \boldsymbol{F(x_a)}) \quad (2)$$

Linearizing the forward model $\boldsymbol{F(x)} = \mathbf{K}\boldsymbol{x} + c$ (c is a constant vector) results in the Jacobian matrix $\mathbf{K}$, which represents the sensitivity of methane concentrations to emissions ($\partial \boldsymbol{y}/\partial \boldsymbol{x}$). The matrix $\mathbf{K}$ is explicitly constructed by performing GEOS-Chem model simulations with individual state vector elements perturbed.

The analytical solution also yields solutions for the posterior error covariance matrix and the averaging kernel matrix:

https://doi.org/10.5194/egusphere-2026-2165
Preprint. Discussion started: 10 June 2026

$$\hat{\mathbf{S}} = (\mathbf{K}^{\mathrm{T}}\mathbf{S}_{\mathbf{O}}^{-1}\mathbf{K} + \mathbf{S}_{\mathbf{a}}^{-1})^{-1} \quad (3)$$

$$\mathbf{A} = \frac{\partial \hat{\boldsymbol{x}}}{\partial \boldsymbol{x}} = \mathbf{I} - \hat{\mathbf{S}}\mathbf{S}_{\mathbf{a}}^{-1} \quad (4)$$

The posterior error covariance matrix ($\hat{\mathbf{S}}$) provides a quantitative measure of the uncertainty associated with the optimized emissions. The averaging kernel matrix ($\mathbf{A}$) describes the sensitivity of the posterior estimate to the true state, with values ranging from 0 (no constraint) to 1 (fully constrained by observations). The trace of matrix $\mathbf{A}$, known as the degree of freedom for signals (DOFS), quantifies the number of independent pieces of information that are effectively constrained by the observing system.

The optimized emissions ($\hat{\boldsymbol{x}}$) can be projected back onto the spatial grid to obtain the distribution of methane fluxes. To assess emissions at the national scale, we further aggregate the posterior fluxes by country. This is achieved by constructing a transformation matrix $\mathbf{W}$ that maps the gridded flux vector ($\hat{\boldsymbol{x}}$) to national totals. The national-level posterior flux ($\hat{\boldsymbol{x}}_{\boldsymbol{country}}$), posterior error covariance matrix ($\hat{\mathbf{S}}_{\mathbf{country}}$), and averaging kernel matrix ($\mathbf{A}_{\mathbf{country}}$) can be calculated as:

$$\hat{\boldsymbol{x}}_{\boldsymbol{country}} = \mathbf{W}\hat{\boldsymbol{x}} \quad (5)$$

$$\hat{\mathbf{S}}_{\mathbf{country}} = \mathbf{W}\hat{\mathbf{S}}\mathbf{W} \quad (6)$$

$$\mathbf{A}_{\mathbf{country}} = \mathbf{I} - \mathbf{W}\hat{\mathbf{S}}\mathbf{W}(\mathbf{W}\mathbf{S}_{\mathbf{a}}\mathbf{W}^{\mathrm{T}})^{-1} \quad (7)$$

The inversion improves the fit to both satellite and surface observations, with reducing root-mean-square errors (Figure S5). In addition, cross-verification of the surface-only and satellite-only inversions shows that each also improves the fit to the other dataset (Figure S6), although only slightly, generally demonstrating the consistency between the two datasets.

We also evaluate the inversion against near-surface vertical gradients derived from independent IAGOS-CARIBIC aircraft observations (Figure S7). Most vertical profile observations are only available over Germany, where IAGOS-CARIBIC aircraft take off or land. Compared to the prior simulation, the posterior captures a sharper concentration gradient between the lower free troposphere and the surface, bringing it into closer agreement with the aircraft observations. This independently supports the upward adjustment in methane emissions from Germany (which creates a sharper near-surface gradient) inferred by the

https://doi.org/10.5194/egusphere-2026-2165
Preprint. Discussion started: 10 June 2026

inversion (see Section 5.1). However, due to the limited availability of such independent observations, we are unable to comprehensively evaluate our inversion against independent data.

3 Observational constraints by satellite and surface observations

Figure 5a presents the spatial distribution of averaging kernel sensitivities across the inversion domain, derived from a joint inversion of satellite and surface observations. The averaging kernel sensitivities, defined as the diagonal elements of the averaging kernel matrix (see Eq. 4), quantify the degree to which the inversion system can independently constrain methane emissions at a given location. A value of zero indicates no observational constraint, while a value of one represents full constraint. The results reveal that methane emissions are not uniformly constrained across the inversion domain. Stronger constraints are observed over central and western Europe (primarily Germany and the Benelux states), whereas eastern and northern regions remain comparatively weakly constrained (Figure 5a). This joint inversion achieves a degree of freedom for signal (DOFS; the sum of the diagonal elements of the averaging kernel matrix, representing the number of independently constrained pieces of information) of 100 for the entire domain, 78 for the European countries, and 67 for the EU-27 countries, with DOFS for individual countries tabulated in Table S1.

To evaluate the respective contributions of satellite and surface observations, we also derived averaging kernel sensitivities from inversions using either satellite or surface observations alone (Figures 5b and 5c; Table S1). The satellite-only inversion yields a DOFS of 31 for the entire domain, 13 for the European countries, and 11 for the EU-27 countries. In contrast, the surface-only inversion yields a DOFS of 77 for the entire domain, 72 for the European countries, and 62 for EU-27, respectively, indicating that surface observations provide most of the observational constraints across Europe. The constraints from surface observations are particularly strong over central and western Europe, where ICOS station density is high, but remain limited over the Iberian Peninsula, southern Italy, and eastern Europe (e.g., Poland and Ukraine), regions with almost no surface data coverage. Satellite data offer little additional information over central and western Europe but provide valuable supplementary constraints over the Iberian Peninsula, eastern Europe, western Russia, and adjacent regions such as Turkey and North Africa. In northern Italy, both satellite and surface observations contribute to constraining emissions. In summary, while the most

https://doi.org/10.5194/egusphere-2026-2165
Preprint. Discussion started: 10 June 2026

effective constraint on European methane emissions comes from the synergistic use of both platforms, the surface network remains the primary driver of the inversion's information content, with satellite observations playing a secondary role that becomes useful in areas poorly covered by ground-based networks.

4 2019–2023 European methane budget

Figure 6 presents the annual anthropogenic methane emissions aggregated across Europe for 2019–2023. The inversion yields a total posterior methane emission of 24.7 Tg a^{-1} from Europe, with 22.1Tg a^{-1} from anthropogenic sources and 2.6 Tg a^{-1} from natural sources. Across anthropogenic sectors, we attribute 11.5 Tg a^{-1} to livestock, 3.9 Tg a^{-1} to landfills, 1.8 Tg a^{-1} to wastewater, 2.0 Tg a^{-1} to natural gas, 0.32 Tg a^{-1} to oil, and 0.89 Tg a^{-1} to coal (Figure 7). The total anthropogenic emissions are on average 1.0 Tg a^{-1} higher than the prior estimate. The largest sectoral adjustment is for livestock, where emissions are increased by about 0.9 Tg a^{-1} (9%) (Figure 7). For natural sources, the inversion reduces the mean estimate from 3.3 Tg a^{-1} to 2.6 Tg a^{-1} (Figure 7).

For the EU-27 countries, the inversion yields a posterior anthropogenic methane emission estimate of 16.7 Tg a^{-1} over 2019–2023, which is 1.2 Tg a^{-1} (8.0%) higher than the prior estimate of 15.5 Tg a^{-1}, indicating an underestimation by the prior inventory. The magnitude of this adjustment is comparable to that inferred for the whole of Europe, suggesting that the revision is primarily driven by corrections within EU member states.

Both prior and posterior estimates show a significant negative trend in total anthropogenic emissions at the continental scale (prior: –0.20 Tg a^{-2}; p = 0.015; posterior: –0.27 Tg a^{-2}; p = 0.03) (Figure 6), indicating that the observational data support an overall decline in European methane emissions. The decrease is primarily driven by reductions in landfill (–0.09 ± 0.03 Tg a^{-2}), coal mining (posterior: –0.09 ± 0.05 Tg a^{-2}), and natural gas (–0.04 ± 0.01 Tg a^{-2}) emissions. In contrast, trends for livestock (–0.01 ± 0.06 Tg a^{-2}) and wastewater (-0.02 ± 0.02 Tg a^{-2}) are insignificant given the uncertainties. We also find a

https://doi.org/10.5194/egusphere-2026-2165
Preprint. Discussion started: 10 June 2026

decrease in wetland emissions of –0.03 ± 0.01 Tg a^{-2} over the study period. For the EU-27, anthropogenic emissions also have decreased (prior: –0.09 Tg a^{-2}, p = 0.10; posterior: –0.11 Tg a^{-2}, p = 0.25), although the trends are not statistically significant.

5 Correction of 2019–2023 mean methane emissions

Figure 8 presents the spatial distribution of posterior methane emissions averaged over the period from 2019 to 2023 and the inversion's corrections relative to prior emissions. Figure 9 summarizes prior and posterior emissions from the top 10 methane emitting countries in Europe, in comparison with their reports to UNFCCC and previous inversion studies. Inversion results for all European countries are also tabulated in Table S1.

5.1 Agriculture and waste dominated regions

We find that the inversion upward adjusts prior methane emissions from the Netherlands, northwestern Germany, and northern Italy (Figure 8). The posterior estimates of anthropogenic emissions for these countries (Germany: 2.78±0.1 Tg a^{-1}; Netherlands: 1.15±0.06 Tg a^{-1}; Italy: 1.87±0.12 Tg a^{-1}) are 27-62% higher than prior estimates (Germany: 2.23 Tg a^{-1}; Netherlands: 0.68 Tg a^{-1}; Italy: 1.40 Tg a^{-1}) and official reports to the UNFCCC (Germany: 1.63 Tg a^{-1}; Netherlands: 0.67 Tg a^{-1}; Italy: 1.68 Tg a^{-1}) (Figure 9). Our posterior estimates are consistent with another inversion by Bruch et al. (2025) using only surface data, but generally deviates from Worden et al. (2022) who used only satellite data and a coarse global model. The upward adjustments in these regions are derived from both of our sensitivity inversions, using either surface or satellite observations alone (Figure S8), although the magnitudes of the corrections differ due to varying observational constraints (Figure 5). This consistency in directions provides additional support that the upward adjustment is robust across different observation platforms in this region.

Based on the relative contribution of each sector in the prior inventory, we attribute most of the upward revision in these countries to the agriculture sector (Figure 10). This attribution is generally supported by recent local-scale studies. For instance, a survey of 51 Dutch dairy farms found that measured whole-farm methane emissions were on average 30% higher than estimates from the Dutch National Inventory (Chen et al., 2025). Conversely, urban emission measurements in several cities

https://doi.org/10.5194/egusphere-2026-2165
Preprint. Discussion started: 10 June 2026

in these countries, including Berlin (Klausner et al., 2020), Groningen, Utrecht, Rotterdam (Tong et al., 2023), and Milan (Cristofanelli et al., 2025), have not shown significant discrepancies when compared to EDGAR or official inventories. Collectively, this suggests that systematic biases may persist in national-level livestock emission accounting, even when using high-tier methodologies that incorporate detailed activity data on animal diet, milk production, and feed use (Bruch et al., 2025; Steiner et al., 2024).

The inversion also indicates moderate upward corrections for anthropogenic emissions across France, Spain, and the terrestrial part of the United Kingdom (Figure 9). The corrections for the UK and France are mainly driven by surface data, whereas the correction for Spain by satellite observations (Figure S7). Posterior emissions are 2.68±0.16 Tg a^{-1} for France and 1.77 ±0.18Tg a^{-1} for Spain, representing an increase of roughly 15% from prior estimates (Figure 9). For the UK, the posterior total emissions (1.58 Tg a^{-1}) remain nearly unchanged from the prior (Figure 9), as the increase over land is offset by decreases in offshore oil and gas emissions over the ocean (see discussion below).

Spatially, the inversion reveals concentrated upward corrections over major urban areas such as Paris, Madrid, and London, alongside weaker, diffuse adjustments likely linked to agricultural sources. Consistent with this finding, recent studies using ground-based (Tu et al. 2022) and satellite-based (Dogniaux et al., 2025) remote sensing have identified landfills as a major, underrepresented methane source in Madrid. Similarly, eddy covariance flux measurements in central London show that urban methane fluxes are substantially underestimated in inventories, with contributions from both biogenic and fossil fuel sources (Helfter et al., 2016).

5.2 Fossil fuel production regions

In addition to agriculture- and waste-related sources, the inversion analysis also revises methane emission estimates for several fossil fuel production regions, including the North Sea and southern Poland. For the North Sea, posterior emissions from offshore oil and gas production are 0.28 Tg a^{-1}, 53.4% lower than prior estimates. This contrasts with a ship-based study (Riddick et al., 2019), which found substantial emissions from UK offshore platforms, suggesting existing inventories may

https://doi.org/10.5194/egusphere-2026-2165
Preprint. Discussion started: 10 June 2026

underestimate. However, those measurements were limited to a short timeframe and may not reflect the variability across different phases of offshore production. This downward adjustment is mainly informed by surface observations, but both satellite- and surface-only inversions agree on its direction (Figure S7).

Over southern Poland, the inversion reveals a revised spatial pattern of emissions within the Upper Silesian Coal Basin (Figure 8), a major production hub accounting for the majority of the EU's hard coal output. Despite this spatial redistribution, the national estimates for all anthropogenic sources and for coal mining methane emissions remain nearly unchanged at 1.7 Tg a^{-1} and 0.41 Tg a^{-1}, respectively (Figure 9 and Figure 10). This result is broadly consistent with extensive multi-scale studies conducted in the region, ranging from individual mine shafts to basin-wide assessments (Andersen et al., 2023; Fiehn et al., 2020; Luther et al., 2019; Luther et al., 2022; Tu et al., 2022).

Other major fossil fuel producers in Europe, such as Romania and Ukraine, show only minor emission adjustments in our atmospheric inversion (Figure 9). This is primarily due to limited capacity of the inversion system to constrain emissions in these regions, as indicated by low observational constraints (DOFS of only 0.77 for Romania and 1.43 for Ukraine). Consequently, while our posterior estimate (0.93 Tg a^{-1}) aligns more closely with the prior EDGAR inventory, it does not conclusively rule out the plausibility of the significantly different UNFCCC value for Ukraine's oil and gas sector (1.9 Tg a^{-1}) (Figure 10). This limitation in observational constraint also explains why our inversion infers no adjustments for Romania (Figure 8), though aircraft-based studies reveal that UNFCCC reports underestimate emissions from the country's southern oil fields (Maazallahi et al., 2025; Kuhlmann et al., 2025).

In Northern Europe, including wetland-rich areas, posterior estimates are generally lower than the prior, implying a possible overestimation of natural and offshore oil and gas emissions. These regional differences reveal localized hotspots or deficits that are not fully captured in the prior inventory. While the prior emissions reproduce broad spatial patterns reasonably well, they may miss finer-scale spatial heterogeneities.

https://doi.org/10.5194/egusphere-2026-2165
Preprint. Discussion started: 10 June 2026

6 Methane emission trends during 2019–2023

To identify the potential effects of recent mitigation policies, we also derived five-year (2019–2023) linear trends in methane emissions from the inversion. These trends are generally uncertain at regional and national scales due to the short time series and large inter-annual variability, but they provide a first indication of broad directional trends in Europe's methane emissions. Figure 11 presents the spatial distribution of prior and posterior methane emission trends from 2019 to 2023. The inversion reveals substantial regional differences in emission trends. Positive emission trends are inferred by the inversion in the Netherlands, Belgium, western Germany, northern Italy, western Poland, and the southern United Kingdom, in contrast to near-zero trends in the prior estimate. Conversely, negative emission trends are observed in southern Poland and eastern Ukraine. In Germany, the Netherlands, Belgium, and other parts of central and western Europe, methane trends are spatially heterogeneous, with increasing emissions potentially associated with agricultural sources (Bruch et al., 2025; Mengistu et al., 2026). However, seasonal variability in fossil fuel and waste treatment sectors may introduce confounding signals that are not fully separable at the current resolution and tracer constraints of our inversion system (Ioannidis et al., 2026). The reductions in southern Poland and eastern Ukraine are attributed to coal-related emission declines (Gajdzik et al., 2024; UNECE, 2024).

Over the North Sea, both the prior and posterior indicate a modest decreasing trend in methane emissions, with the inversion yielding a trend comparable in magnitude to the prior estimate. This suggests limited adjustment by the inversion in this region, likely reflecting relatively weak observational constraints on offshore emissions. Aircraft-based measurements over the southern North Sea have shown that methane emissions from individual offshore facilities are often underestimated by bottom-up inventories (Pühl et al., 2024), suggesting that such facility-level discrepancies may not be readily detectable as regional-scale emission trends in satellite-based inversions.

Figure 12 presents the 2019–2023 anthropogenic methane emission trends for Europe's top 10 emitting countries. Most countries show consistent trend directions between prior and posterior estimates, with differences generally within posterior uncertainties. France, Italy, Germany, and the United Kingdom exhibit stable or small negative trends in prior and posterior estimates, with no statistically significant differences. Romania and Belarus display weak increases in both datasets, reflecting

https://doi.org/10.5194/egusphere-2026-2165
Preprint. Discussion started: 10 June 2026

general agreement. Ukraine shows a consistent decrease but with a stronger posterior trend (–0.09 ± 0.005 Tg a^{-2}) than the prior (–0.05 Tg a^{-2}), suggesting that the prior inventory may underestimate the actual rate of decline. In contrast, the trend directions differ between prior and posterior estimates for countries including the Netherlands, Poland, and Spain. For instance, the Netherlands shifts from a negative (–0.016 Tg a^{-2}) prior trend to a slightly positive (+0.023 ± 0.01 Tg a^{-2}) posterior trend. For Poland and Spain, although the posterior and prior trends are of opposite sign, the posterior uncertainties encompass the prior values, preventing a definitive conclusion on the trend direction.

7 Conclusion

We quantified European methane emissions from 2019–2023 using a joint inversion of satellite (TROPOMI) and ground-based (ICOS) observations. The inversion achieves a DOFS of 100 across the study domain, with the strongest constraints over central and western Europe. These constraints are driven primarily by surface observations (DOFS=77 in the surface-only inversion). Satellite observations contribute comparatively little additional constraints in regions that are already well covered by surface measurements, but they provide valuable complementary information in areas with sparse surface networks, such as the Iberian Peninsula and eastern Europe (DOFS=31 in the satellite-only inversion).

Our inversion yields an average European methane emission of 24.7 Tg a^{-1} for 2019–2023, with anthropogenic sources contributing 22.1 Tg a^{-1}. Sectorally, livestock is the largest contributor (11.5 Tg a^{-1}), followed by landfills (3.9 Tg a^{-1}), wastewater (1.8 Tg a^{-1}), and fossil fuel activities. The posterior anthropogenic total is 1.0 Tg a^{-1} higher than the prior, with the largest upward adjustment (+0.9 Tg a^{-1}) for livestock emissions, while natural source estimates are revised downward. A similar underestimation is found for the EU-27. Both prior and posterior estimates show a declining trend in European anthropogenic emissions, primarily driven by reductions in landfills, coal, and natural gas, whereas trends for livestock and wastewater are statistically insignificant.

The inversion reveals substantial correction patterns over regions dominated by agricultural and waste sources. Substantial upward corrections of 27–62% to prior methane emissions are inferred by the inversion for Germany, the Netherlands, and

https://doi.org/10.5194/egusphere-2026-2165
Preprint. Discussion started: 10 June 2026

Italy. This revision is attributed primarily to underestimated agricultural emissions, a finding consistent with local-scale studies and a recent surface-data inversion. Moderate upward corrections of roughly 15% in France and Spain are likely driven by underestimated urban sources.

The inversion also revises methane emission estimates for key fossil fuel production regions. Over the North Sea, posterior emissions from offshore oil and gas are 53% lower than prior estimates. For southern Poland, the inversion refines the spatial pattern of emissions within the Upper Silesian Coal Basin. In contrast, emissions for Romania and Ukraine are only minimally adjusted due to low observational constraints.

In addition to mean methane emissions, the inversion also reveals trends in methane emissions across Europe from 2019–2023. Notable positive trends are identified in the Netherlands, Belgium, western Germany, northern Italy, western Poland, and the southern United Kingdom, which contrasts with prior estimates. Conversely, declines are observed in southern Poland and eastern Ukraine, linked to sector-specific reductions in coal-related emissions. At the national level, while most top emitters show consistent trend directions between prior and posterior estimates, divergences occur for the Netherlands, Poland, and Spain.

Acknowledgement

We thank the Integrated Carbon Observation System (ICOS) for providing in-situ surface CH_4 observations, the providers of the blended GOSAT+TROPOMI satellite product, and the IAGOS-CARIBIC team for aircraft measurements.

Financial support

This research has been supported by the National Natural Science Foundation of China (grant no. 42577114), the Zhejiang Provincial Natural Science Foundation (grant no. LZJMZ24D050005), and foundation of Westlake University.

https://doi.org/10.5194/egusphere-2026-2165
Preprint. Discussion started: 10 June 2026

References

Andersen, T., Zhao, Z., de Vries, M., Necki, J., Swolkien, J., Menoud, M., Röckmann, T., Roiger, A., Fix, A., Peters, W., and Chen, H.: Local-to-regional methane emissions from the Upper Silesian Coal Basin (USCB) quantified using UAV-based atmospheric measurements, Atmos. Chem. Phys., 23, 5191–5216, https://doi.org/10.5194/acp-23-5191-2023, 2023.

Balasus, N., Jacob, D. J., Lorente, A., Maasakkers, J. D., Parker, R. J., Boesch, H., Chen, Z., Kelp, M. M., Nesser, H., and Varon, D. J.: A blended TROPOMI+GOSAT satellite data product for atmospheric methane using machine learning to correct retrieval biases, Atmos. Meas. Tech., 16, 3787–3807, https://doi.org/10.5194/amt-16-3787-2023, 2023.

Bloom, A. A., Bowman, K. W., Lee, M., Turner, A. J., Schroeder, R., Worden, J. R., Weidner, R., McDonald, K. C., and Jacob, D. J.: A global wetland methane emissions and uncertainty dataset for atmospheric chemical transport models (WetCHARTs version 1.0), Geosci. Model Dev., 10, 2141–2156, https://doi.org/10.5194/gmd-10-2141-2017, 2017.

Brasseur, G. P. and Jacob, D. J.: Modeling of atmospheric chemistry, Cambridge University Press, https://doi.org/10.1017/9781316544754, 2017.

Bruch, V., Rösch, T., Jiménez de la Cuesta Otero, D., Ellerhoff, B., Mamtimin, B., Becker, N., Blechschmidt, A.-M., Förstner, J., and Kaiser-Weiss, A. K.: German methane fluxes in 2021 estimated with an ensemble-enhanced scaling inversion based on the ICON–ART model, EGUsphere [preprint], https://doi.org/10.5194/egusphere-2025-1464, 2025.

Chen, H., Vinković, K., Sun, C., Peters, W., Hensen, A., van der Gon, H. D., van Zanten, M., van den Bulk, P., Velzeboer, I., and van der Zee, T.: A novel approach to rapidly tracking whole-farm methane emissions, Environ. Res. Lett., 20, 034016, 10.1088/1748-9326/adb1f6, 2025.

Chen, Z., Jacob, D. J., Nesser, H., Sulprizio, M. P., Lorente, A., Varon, D. J., Lu, X., Shen, L., Qu, Z., Penn, E., and Yu, X.: Methane emissions from China: a high-resolution inversion of TROPOMI satellite observations, Atmos. Chem. Phys., 22, 10809–10826, https://doi.org/10.5194/acp-22-10809-2022, 2022.

Chen, Z., Jacob, D. J., Gautam, R., Omara, M., Stavins, R. N., Stowe, R. C., Nesser, H., Sulprizio, M. P., Lorente, A., Varon, D. J., Lu, X., Shen, L., Qu, Z., Pendergrass, D. C., and Hancock, S.: Satellite quantification of methane emissions and oil–gas methane intensities from individual countries in the Middle East and North Africa: implications for climate action, Atmos. Chem. Phys., 23, 5945–5967, https://doi.org/10.5194/acp-23-5945-2023, 2023.

https://doi.org/10.5194/egusphere-2026-2165
Preprint. Discussion started: 10 June 2026

Crippa, M., Guizzardi, D., Muntean, M., Schaaf, E., Dentener, F., van Aardenne, J. A., Monni, S., Doering, U., Olivier, J. G. J., Pagliari, V., and Janssens-Maenhout, G.: EDGAR v8.0: Emissions Database for Global Atmospheric Research – Global CH_4 emissions, European Commission, Joint Research Centre (JRC), https://edgar.jrc.ec.europa.eu/dataset_ghg80, 2023.

Cristofanelli, P., Zannoni, N., Apadula, F., Barnaba, F., Bracci, A., Bellini, A., Calzolari, F., Diliberto, L., Manca, G., and Mardonez, V.: Urban CO2 and CH4 atmospheric measurements in the Milan city area (northern Italy), EGU General Assembly Conference Abstracts, EGU25-17963,

Deng, Z., Ciais, P., Tzompa-Sosa, Z. A., Saunois, M., Qiu, C., Tan, C., Sun, T., Ke, P., Cui, Y., Tanaka, K., Lin, X., Thompson, R. L., Tian, H., Yao, Y., Huang, Y., Lauerwald, R., Jain, A. K., Xu, X., Bastos, A., Sitch, S., Palmer, P. I., Lauvaux, T., d'Aspremont, A., Giron, C., Benoit, A., Poulter, B., Chang, J., Petrescu, A. M. R., Davis, S. J., Liu, Z., Grassi, G., Albergel, C., Tubiello, F. N., Perugini, L., Peters, W., and Chevallier, F.: Comparing national greenhouse gas budgets reported in UNFCCC inventories against atmospheric inversions, Earth Syst. Sci. Data, 14, 1639–1675, https://doi.org/10.5194/essd-14-1639-2022, 2022.

Dogniaux, M., Maasakkers, J. D., Girard, M., Jervis, D., McKeever, J., Schuit, B. J., Sharma, S., Lopez-Noreña, A., Varon, D. J., and Aben, I.: Global satellite survey reveals uncertainty in landfill methane emissions, Nature, 647, 397-402, 10.1038/s41586-025-09683-8, 2025.

EEA, 2024. Annual European Union greenhouse gas inventory 1990–2022 and inventory report 2024. European Environment Agency.

European Commission: About the Global Methane Pledge, available at: https://www.globalmethanepledge.org/, last access: 1 July 2025, 2021.

European Union. Regulation (EU) 2024/1787 of the European Parliament and of the Council of 13 June 2024 on the reduction of methane emissions in the energy sector and amending Regulation (EU) 2019/942. Official Journal of the European Union, L, 2024/1787, 2024.

Fiehn, A., Kostinek, J., Eckl, M., Klausner, T., Gałkowski, M., Chen, J., Gerbig, C., Röckmann, T., Maazallahi, H., Schmidt, M., Korbeń, P., Nęcki, J., Jagoda, P., Wildmann, N., Mallaun, C., Bun, R., Nickl, A.-L., Jöckel, P., Fix, A., and Roiger,

https://doi.org/10.5194/egusphere-2026-2165
Preprint. Discussion started: 10 June 2026

A.: Estimating CH4, CO2 and CO emissions from coal mining and industrial activities in the Upper Silesian Coal Basin using an aircraft-based mass balance approach, Atmos. Chem. Phys., 20, 12675–12695, https://doi.org/10.5194/acp-20-12675-2020, 2020.

Fu, B., Jiang, Y., Chen, G., Lu, M., Lai, Y., Suo, X., and Li, B.: Unraveling the dynamics of atmospheric methane: the impact of anthropogenic and natural emissions, Environ. Res. Lett., 19, 064001, 10.1088/1748-9326/ad4617, 2024.

Fung, I. Y., John, J. G., Lerner, J., Matthews, E., Prather, M. J., Steele, L. P., and Fraser, P. J.: Three dimensional model synthesis of the global methane cycle, J. Geophys. Res., 96, 13033–13065, https://doi.org/10.1029/91JD01247, 1991.

Gajdzik, B., Tobór-Osadnik, K., Wolniak, R., and Grebski, W. W.: European Climate Policy in the Context of the Problem of Methane Emissions from Coal Mines in Poland, 10.3390/en17102396, 2024.

Gelaro, R., McCarty, W., Suárez, M. J., Todling, R., Molod, A., Takacs, L., Randles, C. A., Darmenov, A., Bosilovich, M. G., Reichle, R., Wargan, K., Coy, L., Cullather, R., Draper, C., Akella, S., Buchard, V., Conaty, A., da Silva, A. M., Gu, W., Kim, G.-K., Koster, R., Lucchesi, R., Merkova, D., Nielsen, J. E., Partyka, G., Pawson, S., Putman, W., Rienecker, M., Schubert, S. D., Sienkiewicz, M., and Zhao, B.: The Modern-Era Retrospective Analysis for Research and Applications, Version 2 (MERRA-2), J. Climate, 30, 5419–5454, https://doi.org/10.1175/JCLI-D-16-0758.1, 2017.

Hancock, S. E., Jacob, D., Chen, Z., Nesser, H., Davitt, A., Varon, D. J., Sulprizio, M. P., Balasus, N., Estrada, L. A., East, J. D., Penn, E., Randles, C. A., Worden, J., Aben, I., Parker, R. J., and Maasakkers, J. D.: Satellite quantification of methane emissions from South American countries: A high-resolution inversion of TROPOMI and GOSAT observations, EGUsphere [preprint], https://doi.org/10.5194/egusphere-2024-1763, 2024.

Hasekamp, O., Lorente, A., Hu, H., Butz, A., aan de Brugh, J., and Landgraf, J.: Algorithm Theoretical Baseline Document for Sentinel-5 Precursor Methane Retrieval, available at: https://sentinels.copernicus.eu/documents/247904/2476257/Sentinel-5P-TROPOMI-ATBD-Methane-retrieval.pdf, last access: 31 August 2025.

Helfter, C., Tremper, A. H., Halios, C. H., Kotthaus, S., Bjorkegren, A., Grimmond, C. S. B., Barlow, J. F., and Nemitz, E.: Spatial and temporal variability of urban fluxes of methane, carbon monoxide and carbon dioxide above London, UK, Atmos. Chem. Phys., 16, 10543–10557, https://doi.org/10.5194/acp-16-10543-2016, 2016.

https://doi.org/10.5194/egusphere-2026-2165
Preprint. Discussion started: 10 June 2026

Houweling, S., Bergamaschi, P., Chevallier, F., Heimann, M., Kaminski, T., Krol, M., Michalak, A. M., and Patra, P.: Global inverse modeling of CH4 sources and sinks: an overview of methods, Atmos. Chem. Phys., 17, 235–256, https://doi.org/10.5194/acp-17-235-2017, 2017.

Hu, H., Hasekamp, O., Butz, A., Galli, A., Landgraf, J., Aan de Brugh, J., Borsdorff, T., Scheepmaker, R., and Aben, I.: The operational methane retrieval algorithm for TROPOMI, Atmos. Meas. Tech., 9, 5423–5440, https://doi.org/10.5194/amt-9-5423-2016, 2016.

ICOS RI, Apadula, F., Arnold, S., Bergamaschi, P., Biermann, T., Chen, H., Colomb, A., Conil, S., Couret, C., Cristofanelli, P., De Mazière, M., Delmotte, M., Di Iorio, T., Emmenegger, L., Forster, G., Frumau, A., Harris, E., Haszpra, L., Hatakka, J., Heliasz, M., Heltai, D., Hensen, A., Hermansen, O., Hoheisel, A., Kneuer, T., Komínková, K., Kubistin, D., Larmanou, E., Laurent, O., Laurila, T., Lehner, I., Lehtinen, K., Leskinen, A., Leuenberger, M., Levula, J., Lindauer, M., Lopez, M., Lund Myhre, C., Lunder, C., Mammarella, I., Manca, G., Manning, A., Marek, M.V., Marklund, P., Meinhardt, F., Miettinen, P., Molnár, M., Montaguti, S., Mölder, M., Müller-Williams, J., O'Doherty, S., Ottosson-Löfvenius, M., Piacentino, S., Pichon, J.-M., Pitt, J., Platt, S.M., Plaß-Dülmer, C., Ramonet, M., Rivas-Soriano, P., Roulet, Y.-A., Scheeren, B., Schmidt, M., Schumacher, M., Sferlazzo, D., Sha, M.K., Smith, P., Stanley, K., Steinbacher, M., Sørensen, L.L., Trisolino, P., Vítková, G., Ylisirniö, A., Yver-Kwok, C., Zazzeri, G., Zwerschke, E., di Sarra, A., ICOS ATC-Laboratoires des Sciences du Climat et de L'Environnement (LSCE), France, ICOS Central Radiocarbon Laboratory (CRL), Germany, ICOS Flask And Calibration Laboratory (FCL), Germany, 2025. ICOS Atmosphere Release 2025-1 of Level 2 Greenhouse Gas Mole Fractions of CO2, CH4, N2O, CO, meteorology and 14CO2, and flask samples analysed for CO2, CH4, N2O, CO, H2, SF6, delta 13C CO2, delta18OCO2, delta O2N2 and 14C. https://doi.org/10.18160/PP29-9CNZ.

Ioannidis, E., Meesters, A., Steiner, M., Brunner, D., Reum, F., Pison, I., Berchet, A., Thompson, R., Sollum, E., Koch, F.-T., Gerbig, C., Wang, F., Maksyutov, S., Tsuruta, A., Tenkanen, M., Aalto, T., Monteil, G., Lin, H., Ren, G., Scholze, M., and Houweling, S.: An inter-comparison of inverse models for estimating European CH4 emissions, Earth Syst. Sci. Data, 18, 167–198, https://doi.org/10.5194/essd-18-167-2026, 2026.

https://doi.org/10.5194/egusphere-2026-2165
Preprint. Discussion started: 10 June 2026

IPCC: Climate Change 2021: The Physical Science Basis, Contribution of Working Group I to the Sixth Assessment Report of the Intergovernmental Panel on Climate Change, Cambridge University Press, https://doi.org/10.1017/9781009157896, 2021.

Jacob, D. J., Varon, D. J., Cusworth, D. H., Dennison, P. E., Frankenberg, C., Gautam, R., Guanter, L., Kelley, J., McKeever, J., Ott, L. E., Poulter, B., Qu, Z., Thorpe, A. K., Worden, J. R., and Duren, R. M.: Quantifying methane emissions from the global scale down to point sources using satellite observations of atmospheric methane, Atmos. Chem. Phys., 22, 9617–9646, https://doi.org/10.5194/acp-22-9617-2022, 2022.

Kirschke, S., Bousquet, P., Ciais, P., Saunois, M., Canadell, J. G., Dlugokencky, E. J., Bergamaschi, P., Bergmann, D., Blake, D. R., Bruhwiler, L., Cameron Smith, P., Castaldi, S., Chevallier, F., Feng, L., Fraser, A., Heimann, M., Hodson, E. L., Houweling, S., Josse, B., Fraser, P. J., Krummel, P. B., Lamarque, J., Langenfelds, R. L., Le Quéré, C., Naik, V., O'Doherty, S., Palmer, P. I., Pison, I., Plummer, D., Poulter, B., Prinn, R. G., Rigby, M., Ringeval, B., Santini, M., Schmidt, M., Shindell, D. T., Simpson, I. J., Spahni, R., Steele, L. P., Strode, S. A., Sudo, K., Szopa, S., van der Werf, G. R., Voulgarakis, A., van Weele, M., Weiss, R. F., Williams, J. E., and Zeng, G.: Three decades of global methane sources and sinks, Nat. Geosci., 6, 813–823, 2013.

Klausner, T., Mertens, M., Huntrieser, H., Galkowski, M., Kuhlmann, G., Baumann, R., Fiehn, A., Jöckel, P., Pühl, M., and Roiger, A.: Urban greenhouse gas emissions from the Berlin area: A case study using airborne CO2 and CH4 in situ observations in summer 2018, Elementa: Science of the Anthropocene, 8, 15, 10.1525/elementa.411, 2020.

Kuhlmann, G., Stavropoulou, F., Schwietzke, S., Zavala-Araiza, D., Thorpe, A., Hueni, A., Emmenegger, L., Calcan, A., Röckmann, T., and Brunner, D.: Evidence of successful methane mitigation in one of Europe's most important oil production region, Atmos. Chem. Phys., 25, 5371–5385, https://doi.org/10.5194/acp-25-5371-2025, 2025.

Liang, R., Zhang, Y., Chen, W., Zhang, P., Liu, J., Chen, C., Mao, H., Shen, G., Qu, Z., Chen, Z., Zhou, M., Wang, P., Parker, R. J., Boesch, H., Lorente, A., Maasakkers, J. D., and Aben, I.: East Asian methane emissions inferred from high-resolution inversions of GOSAT and TROPOMI observations: a comparative and evaluative analysis, Atmos. Chem. Phys., 23, 8039–8057, https://doi.org/10.5194/acp-23-8039-2023, 2023.

https://doi.org/10.5194/egusphere-2026-2165
Preprint. Discussion started: 10 June 2026

Liang, R., Zhang, Y., Hu, Q., Li, T., Li, S., Yuan, W., Xu, J., Zhao, Y., Zhang, P., Chen, W., Zhuang, M., Shen, G., and Chen, Z.: Satellite-Based Monitoring of Methane Emissions from China's Rice Hub, Environ. Sci. Technol., 58, 23127-23137, 10.1021/acs.est.4c09822, 2024.

Lu, X., Jacob, D. J., Wang, H., Maasakkers, J. D., Zhang, Y., Scarpelli, T. R., Shen, L., Qu, Z., Sulprizio, M. P., Nesser, H., Bloom, A. A., Ma, S., Worden, J. R., Fan, S., Parker, R. J., Boesch, H., Gautam, R., Gordon, D., Moran, M. D., Reuland, F., Villasana, C. A. O., and Andrews, A.: Methane emissions in the United States, Canada, and Mexico: evaluation of national methane emission inventories and 2010–2017 sectoral trends by inverse analysis of in situ (GLOBALVIEWplus CH4 ObsPack) and satellite (GOSAT) atmospheric observations, Atmos. Chem. Phys., 22, 395–418, https://doi.org/10.5194/acp-22-395-2022, 2022.

Luther, A., Kleinschek, R., Scheidweiler, L., Defratyka, S., Stanisavljevic, M., Forstmaier, A., Dandocsi, A., Wolff, S., Dubravica, D., Wildmann, N., Kostinek, J., Jöckel, P., Nickl, A.-L., Klausner, T., Hase, F., Frey, M., Chen, J., Dietrich, F., Nęcki, J., Swolkień, J., Fix, A., Roiger, A., and Butz, A.: Quantifying CH4 emissions from hard coal mines using mobile sun-viewing Fourier transform spectrometry, Atmos. Meas. Tech., 12, 5217–5230, https://doi.org/10.5194/amt-12-5217-2019, 2019.

Luther, A., Kostinek, J., Kleinschek, R., Defratyka, S., Stanisavljević, M., Forstmaier, A., Dandocsi, A., Scheidweiler, L., Dubravica, D., Wildmann, N., Hase, F., Frey, M. M., Chen, J., Dietrich, F., Nęcki, J., Swolkień, J., Knote , C., Vardag, S. N., Roiger, A., and Butz, A.: Observational constraints on methane emissions from Polish coal mines using a ground-based remote sensing network, Atmos. Chem. Phys., 22, 5859–5876, https://doi.org/10.5194/acp-22-5859-2022, 2022.

Lu, X., Jacob, D. J., Zhang, Y., Shen, L., Sulprizio, M. P., Maasakkers, J. D., Varon, D. J., Qu, Z., Chen, Z., Hmiel, B., Parker, R. J., Boesch, H., Wang, H., He, C., and Fan, S.: Observation-derived 2010-2019 trends in methane emissions and intensities from US oil and gas fields tied to activity metrics, Proc. Natl. Acad. Sci. U.S.A., 120, e2217900120, 10.1073/pnas.2217900120, 2023.

Maazallahi, H., Stavropoulou, F., Sutanto, S. J., Steiner, M., Brunner, D., Mertens, M., Jöckel, P., Visschedijk, A., Denier van der Gon, H., Dellaert, S., Velandia Salinas, N., Schwietzke, S., Zavala-Araiza, D., Ghemulet, S., Pana, A., Ardelean, M., Corbu, M., Calcan, A., Conley, S. A., Smith, M. L., and Röckmann, T.: Airborne in situ quantification of methane

https://doi.org/10.5194/egusphere-2026-2165
Preprint. Discussion started: 10 June 2026

emissions from oil and gas production in Romania, Atmos. Chem. Phys., 25, 1497–1511, https://doi.org/10.5194/acp-25-1497-2025, 2025.

Maasakkers, J. D., Jacob, D. J., Sulprizio, M. P., Scarpelli, T. R., Nesser, H., Sheng, J.-X., Zhang, Y., Hersher, M., Bloom, A. A., Bowman, K. W., Worden, J. R., Janssens-Maenhout, G., and Parker, R. J.: Global distribution of methane emissions, emission trends, and OH concentrations and trends inferred from an inversion of GOSAT satellite data for 2010–2015, Atmos. Chem. Phys., 19, 7859–7881, https://doi.org/10.5194/acp-19-7859-2019, 2019.

Maasakkers, J. D., Jacob, D. J., Sulprizio, M. P., Scarpelli, T. R., Nesser, H., Sheng, J., Zhang, Y., Lu, X., Bloom, A. A., Bowman, K. W., Worden, J. R., and Parker, R. J.: 2010–2015 North American methane emissions, sectoral contributions, and trends: a high-resolution inversion of GOSAT observations of atmospheric methane, Atmos. Chem. Phys., 21, 4339–4356, https://doi.org/10.5194/acp-21-4339-2021, 2021.

Manning, A. J., O'Doherty, S., Jones, A. R., Simmonds, P. G., and Derwent, R. G.: Estimating UK methane and nitrous oxide emissions from 1990 to 2007 using an inversion modeling approach, Journal of Geophysical Research: Atmospheres, 116, https://doi.org/10.1029/2010JD014763, 2011.

Mengistu, A. G., Tsuruta, A., Berchet, A., Thompson, R., Tenkanen, M., Lindqvist, H., Markkanen, T., Leppänen, A., Laitinen, A., Martinez, A., Fortems-Cheiney, A., Höglund-Isaksson, L., and Aalto, T.: High-resolution inversion of methane emissions over Europe using the Community Inversion Framework and FLEXPART, EGUsphere [preprint], https://doi.org/10.5194/egusphere-2025-5877, 2026.

Nisbet, E. G., Fisher, R. E., Lowry, D., France, J. L., Allen, G., Bakkaloglu, S., Broderick, T. J., Cain, M., Coleman, M., Fernandez, J., Forster, G., Griffiths, P. T., Iverach, C. P., Kelly, B. F. J., Manning, M. R., Nisbet-Jones, P. B. R., Pyle, J. A., Townsend-Small, A., al-Shalaan, A., Warwick, N., and Zazzeri, G.: Methane Mitigation: Methods to Reduce Emissions, on the Path to the Paris Agreement, Rev. Geophys., 58, e2019RG000675, https://doi.org/10.1029/2019RG000675, 2020.

Pison, I., Berchet, A., Saunois, M., Bousquet, P., Broquet, G., Conil, S., Delmotte, M., Ganesan, A., Laurent, O., Martin, D., O'Doherty, S., Ramonet, M., Spain, T. G., Vermeulen, A., and Yver Kwok, C.: How a European network may help with

https://doi.org/10.5194/egusphere-2026-2165
Preprint. Discussion started: 10 June 2026

estimating methane emissions on the French national scale, Atmos. Chem. Phys., 18, 3779–3798, https://doi.org/10.5194/acp-18-3779-2018, 2018.

Pühl, M., Roiger, A., Fiehn, A., Gorchov Negron, A. M., Kort, E. A., Schwietzke, S., Pisso, I., Foulds, A., Lee, J., France, J. L., Jones, A. E., Lowry, D., Fisher, R. E., Huang, L., Shaw, J., Bateson, P., Andrews, S., Young, S., Dominutti, P., Lachlan-Cope, T., Weiss, A., and Allen, G.: Aircraft-based mass balance estimate of methane emissions from offshore gas facilities in the southern North Sea, Atmos. Chem. Phys., 24, 1005–1024, https://doi.org/10.5194/acp-24-1005-2024, 2024.

Prather, M. J., Holmes, C. D., and Hsu, J.: Reactive greenhouse gas scenarios: Systematic exploration of uncertainties and the role of atmospheric chemistry, Geophys. Res. Lett., 39, L09803, https://doi.org/10.1029/2012GL051440, 2012.

Qu, Z., Jacob, D. J., Shen, L., Lu, X., Zhang, Y., Scarpelli, T. R., Nesser, H., Sulprizio, M. P., Maasakkers, J. D., Bloom, A. A., Worden, J. R., Parker, R. J., and Delgado, A. L.: Global distribution of methane emissions: a comparative inverse analysis of observations from the TROPOMI and GOSAT satellite instruments, Atmos. Chem. Phys., 21, 14159–14175, https://doi.org/10.5194/acp-21-14159-2021, 2021.

Riddick, S. N., Mauzerall, D. L., Celia, M., Harris, N. R. P., Allen, G., Pitt, J., Staunton-Sykes, J., Forster, G. L., Kang, M., Lowry, D., Nisbet, E. G., and Manning, A. J.: Methane emissions from oil and gas platforms in the North Sea, Atmos. Chem. Phys., 19, 9787–9796, https://doi.org/10.5194/acp-19-9787-2019, 2019.

Saunois, M., Stavert, A. R., Poulter, B., Bousquet, P., Canadell, J. G., Jackson, R. B., Raymond, P. A., Dlugokencky, E. J., Houweling, S., Patra, P. K., Ciais, P., Arora, V. K., Bastviken, D., Bergamaschi, P., Blake, D. R., Brailsford, G., Bruhwiler, L., Carlson, K. M., Carrol, M., Castaldi, S., Chandra, N., Crevoisier, C., Crill, P. M., Covey, K., Curry, C. L., Etiope, G., Frankenberg, C., Gedney, N., Hegglin, M. I., Höglund-Isaksson, L., Hugelius, G., Ishizawa, M., Ito, A., Janssens-Maenhout, G., Jensen, K. M., Joos, F., Kleinen, T., Krummel, P. B., Langenfelds, R. L., Laruelle, G. G., Liu, L., Machida, T., Maksyutov, S., McDonald, K. C., McNorton, J., Miller, P. A., Melton, J. R., Morino, I., Müller, J., Murguia-Flores, F., Naik, V., Niwa, Y., Noce, S., O'Doherty, S., Parker, R. J., Peng, C., Peng, S., Peters, G. P., Prigent, C., Prinn, R., Ramonet, M., Regnier, P., Riley, W. J., Rosentreter, J. A., Segers, A., Simpson, I. J., Shi, H., Smith, S. J., Steele, L. P., Thornton, B. F., Tian, H., Tohjima, Y., Tubiello, F. N., Tsuruta, A., Viovy, N., Voulgarakis, A., Weber, T. S., van Weele,

https://doi.org/10.5194/egusphere-2026-2165
Preprint. Discussion started: 10 June 2026

M., van der Werf, G. R., Weiss, R. F., Worthy, D., Wunch, D., Yin, Y., Yoshida, Y., Zhang, W., Zhang, Z., Zhao, Y., Zheng, B., Zhu, Q., Zhu, Q., and Zhuang, Q.: The Global Methane Budget 2000–2017, Earth Syst. Sci. Data, 12, 1561–1623, https://doi.org/10.5194/essd-12-1561-2020, 2020.

Shen, L., Zavala-Araiza, D., Gautam, R., Omara, M., Scarpelli, T., Sheng, J., Sulprizio, M. P., Zhuang, J., Zhang, Y., Qu, Z., and Lu, X.: Unravelling a large methane emission discrepancy in Mexico using satellite observations, Remote Sens. Environ., 260, 112461, https://doi.org/10.1016/j.rse.2021.112461, 2021.

Shen, L., Gautam, R., Omara, M., Zavala-Araiza, D., Maasakkers, J. D., Scarpelli, T. R., Lorente, A., Lyon, D., Sheng, J., Varon, D. J., Nesser, H., Qu, Z., Lu, X., Sulprizio, M. P., Hamburg, S. P., and Jacob, D. J.: Satellite quantification of oil and natural gas methane emissions in the US and Canada including contributions from individual basins, Atmos. Chem. Phys., 22, 11203–11215, https://doi.org/10.5194/acp-22-11203-2022, 2022.

Shen, L., Jacob, D. J., Gautam, R., Omara, M., Scarpelli, T. R., Lorente, A., Zavala-Araiza, D., Lu, X., Chen, Z., and Lin, J.: National quantifications of methane emissions from fuel exploitation using high resolution inversions of satellite observations, Nat. Commun., 14, 4948, 10.1038/s41467-023-40671-6, 2023.

Steiner, M., Peters, W., Luijkx, I., Henne, S., Chen, H., Hammer, S., and Brunner, D.: European CH4 inversions with ICON-ART coupled to the CarbonTracker Data Assimilation Shell, Atmos. Chem. Phys., 24, 2759–2782, https://doi.org/10.5194/acp-24-2759-2024, 2024.

Szopa, S., Naik, V., Adhikary, B., Artaxo, P., Berntsen, T., Collins, W. D., Fuzzi, S., Gallardo, L., Kiendler-Scharr, A., Klimont, Z., Liao, H., Unger, N., and Zanis, P.: Short-Lived Climate Forcers, in: Climate Change: The Physical Science Basis. Contribution of Working Group I to the Sixth Assessment Report of the Intergovernmental Panel on Climate Change, edited by: Masson-Delmotte, V., Zhai, P., Pirani, A., Connors, S. L., Péan, C., Berger, S., Caud, N., Chen, Y., Goldfarb, L., Gomis, M. I., Huang, M., Leitzell, K., Lonnoy, E., Matthews, J. B. R., Maycock, T. K., Waterfield, T., Yelekçi, O., Yu, R., and Zhou, B., Cambridge University Press, Cambridge, United Kingdom and New York, NY, USA, 817–922, https://doi.org/10.1017/9781009157896.008, 2021.

Tong, X., van Heuven, S., Scheeren, B., Kers, B., Hutjes, R., and Chen, H.: Aircraft-Based AirCore Sampling for Estimates of N2O and CH4 Emissions, Environmental Science & Technology, 57, 15571-15579, 10.1021/acs.est.3c04932, 2023.

https://doi.org/10.5194/egusphere-2026-2165
Preprint. Discussion started: 10 June 2026

Tu, Q., Schneider, M., Hase, F., Khosrawi, F., Ertl, B., Necki, J., Dubravica, D., Diekmann, C. J., Blumenstock, T., and Fang, D.: Quantifying CH4 emissions in hard coal mines from TROPOMI and IASI observations using the wind-assigned anomaly method, Atmos. Chem. Phys., 22, 9747–9765, https://doi.org/10.5194/acp-22-9747-2022, 2022.

Turner, A. J. and Jacob, D. J.: Balancing aggregation and smoothing errors in inverse models, Atmos. Chem. Phys., 15, 7039–7048, https://doi.org/10.5194/acp-15-7039-2015, 2015a.

Turner, A. J., Jacob, D. J., Wecht, K. J., Maasakkers, J. D., Lundgren, E., Andrews, A. E., Biraud, S. C., Boesch, H., Bowman, K. W., Deutscher, N. M., Dubey, M. K., Griffith, D. W. T., Hase, F., Kuze, A., Notholt, J., Ohyama, H., Parker, R., Payne, V. H., Sussmann, R., Sweeney, C., Velazco, V. A., Warneke, T., Wennberg, P. O., and Wunch, D.: Estimating global and North American methane emissions with high spatial resolution using GOSAT satellite data, Atmos. Chem. Phys., 15, 7049–7069, https://doi.org/10.5194/acp-15-7049-2015, 2015b.

UNECE (2024). International Workshop on Best Practices in Coal Mine Methane Monitoring, Capture, and Use, Workshop Summary and Highlights, Katowice, 5–6 November 2024.

Veefkind, J. P., Aben, I., McMullan, K., Förster, H., de Vries, J., Otter, G., Claas, J., Eskes, H. J., de Haan, J. F., Kleipool, Q., van Weele, M., Hasekamp, O., Hoogeveen, R., Landgraf, J., Snel, R., Tol, P., Ingmann, P., Voors, R., Kruizinga, B., Vink, R., Visser, H., and Levelt, P. F.: TROPOMI on the ESA Sentinel-5 Precursor: A GMES mission for global observations of the atmospheric composition for climate, air quality and ozone layer applications, Remote Sens. Environ., 120, 70–83, https://doi.org/10.1016/j.rse.2011.09.027, 2012.

Wang, Y., Zhang, Y., Tian, X., Wang, X., Yuan, W., Ding, J., Jiang, F., Jin, Z., Ju, W., Liang, R., Lu, X., Shen, L., Sun, S., Wang, T., Zhang, H., Zhao, M., and Piao, S.: Towards verifying and improving estimations of China's CO2 and CH4 budgets using atmospheric inversions, National Science Review, 12, nwaf090, 10.1093/nsr/nwaf090, 2025.

Wecht, K. J., Jacob, D. J., Frankenberg, C., Jiang, Z., and Blake, D. R.: Mapping of North American methane emissions with high spatial resolution by inversion of SCIAMACHY satellite data, J. Geophys. Res.-Atmos., 119, 7741–7756, https://doi.org/10.1002/2014JD021551, 2014.

Worden, J. R., Cusworth, D. H., Qu, Z., Yin, Y., Zhang, Y., Bloom, A. A., Ma, S., Byrne, B. K., Scarpelli, T., Maasakkers, J. D., Crisp, D., Duren, R., and Jacob, D. J.: The 2019 methane budget and uncertainties at 1° resolution and each country

https://doi.org/10.5194/egusphere-2026-2165
Preprint. Discussion started: 10 June 2026

through Bayesian integration Of GOSAT total column methane data and a priori inventory estimates, Atmos. Chem. Phys., 22, 6811–6841, https://doi.org/10.5194/acp-22-6811-2022, 2022.

Zhang, P., Zhang, Y., and Liang, R.: Correction of Simulation Biases in Stratospheric Methane Concentrations for the Inverse Analysis of Satellite Column Observations, Journal of Geophysical Research: Atmospheres, 130, e2024JD042596, https://doi.org/10.1029/2024JD042596, 2025.

Zhang, Y., Gautam, R., Pandey, S., Omara, M., Maasakkers, J. D., Sadavarte, P., Lyon, D., Nesser, H., Sulprizio, M. P., Varon, D. J., and Zhang, R.: Quantifying methane emissions from the largest oil-producing basin in the United States from space, Sci. Adv., 6, eaaz5120, https://doi.org/10.1126/sciadv.aaz5120, 2020.

Zhang, Y., Jacob, D. J., Lu, X., Maasakkers, J. D., Scarpelli, T. R., Sheng, J.-X., Shen, L., Qu, Z., Sulprizio, M. P., Chang, J., Bloom, A. A., Ma, S., Worden, J., Parker, R. J., and Boesch, H.: Attribution of the accelerating increase in atmospheric methane during 2010–2018 by inverse analysis of GOSAT observations, Atmos. Chem. Phys., 21, 3643–3666, https://doi.org/10.5194/acp-21-3643-2021, 2021.

Zhang, Y., Fang, S., Chen, J., Lin, Y., Chen, Y., Liang, R., Jiang, K., Parker, R. J., Boesch, H., Steinbacher, M., Sheng, J.-X., Lu, X., Song, S., and Peng, S.: Observed changes in China's methane emissions linked to policy drivers, Proc. Natl. Acad. Sci. U.S.A., 119, e2202742119, https://doi.org/10.1073/pnas.2202742119, 2022.

Zhang, Z., Poulter, B., Feldman, A. F., Ying, Q., Ciais, P., Peng, S., and Li, X.: Recent intensification of wetland methane feedback, Nat. Clim. Chang, 13, 430-433, 10.1038/s41558-023-01629-0, 2023.

https://doi.org/10.5194/egusphere-2026-2165
Preprint. Discussion started: 10 June 2026

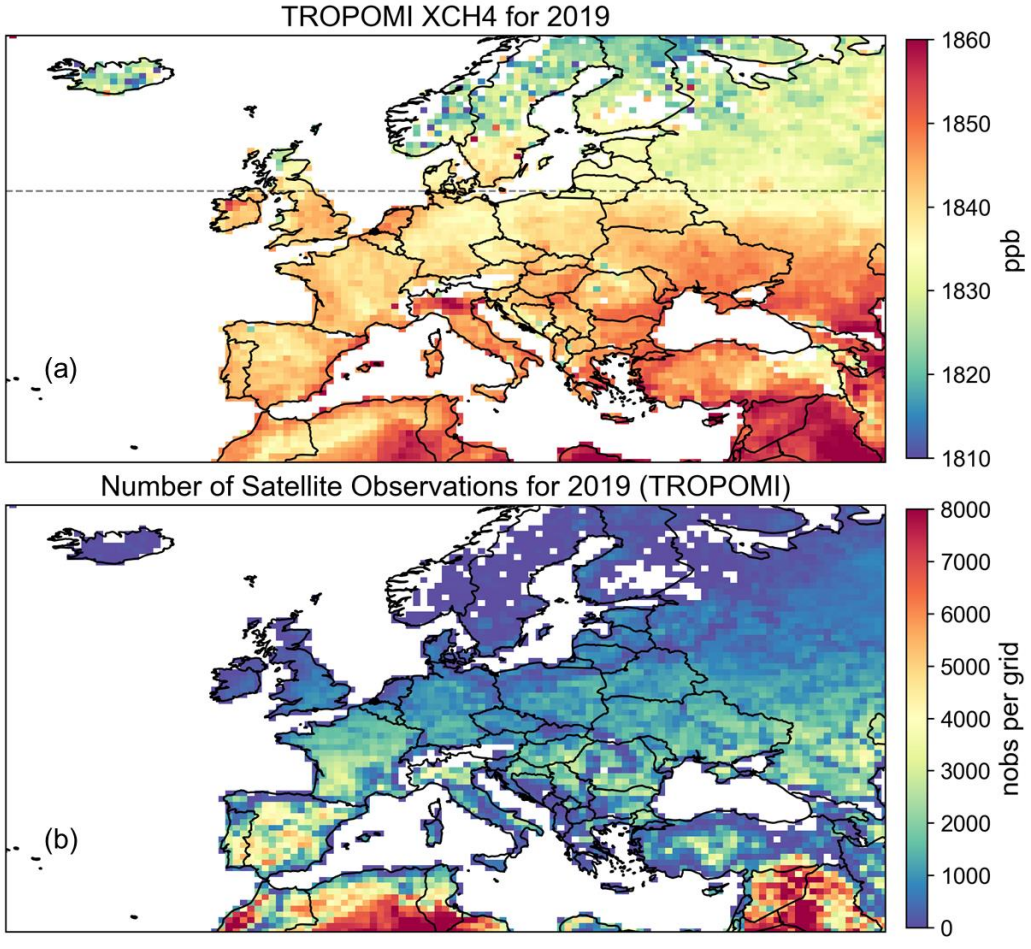

Figure 1: TROPOMI satellite observations. (a) Spatial distribution of annual average TROPOMI methane column-averaged mixing ratios over Europe for 2019. Observational data constraints for the inversion are shown below the black dashed line. (b) Spatial distribution of the number of TROPOMI observations for 2019. Data are plotted in a 0.5°×0.625° grid.

https://doi.org/10.5194/egusphere-2026-2165
Preprint. Discussion started: 10 June 2026

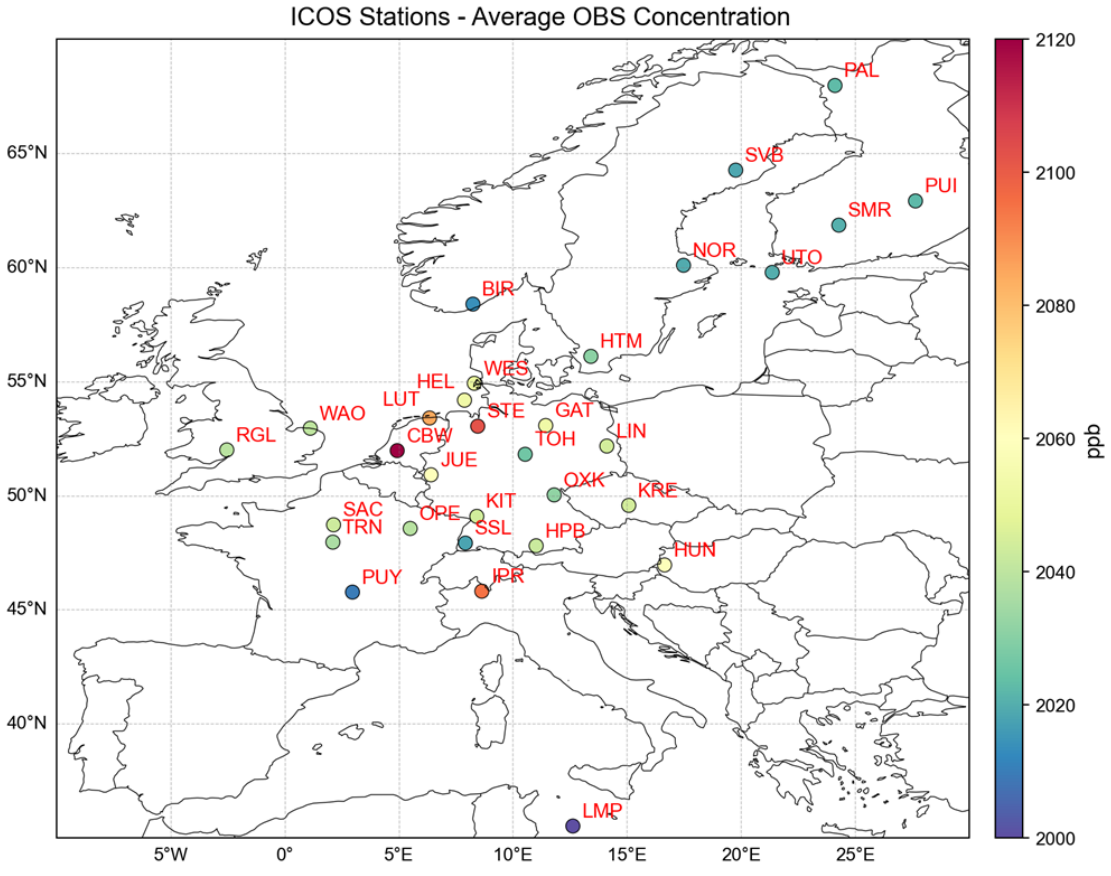

Figure 2: ICOS surface observations. Site locations and their 2019–2023 daytime average concentrations are shown.

https://doi.org/10.5194/egusphere-2026-2165
Preprint. Discussion started: 10 June 2026

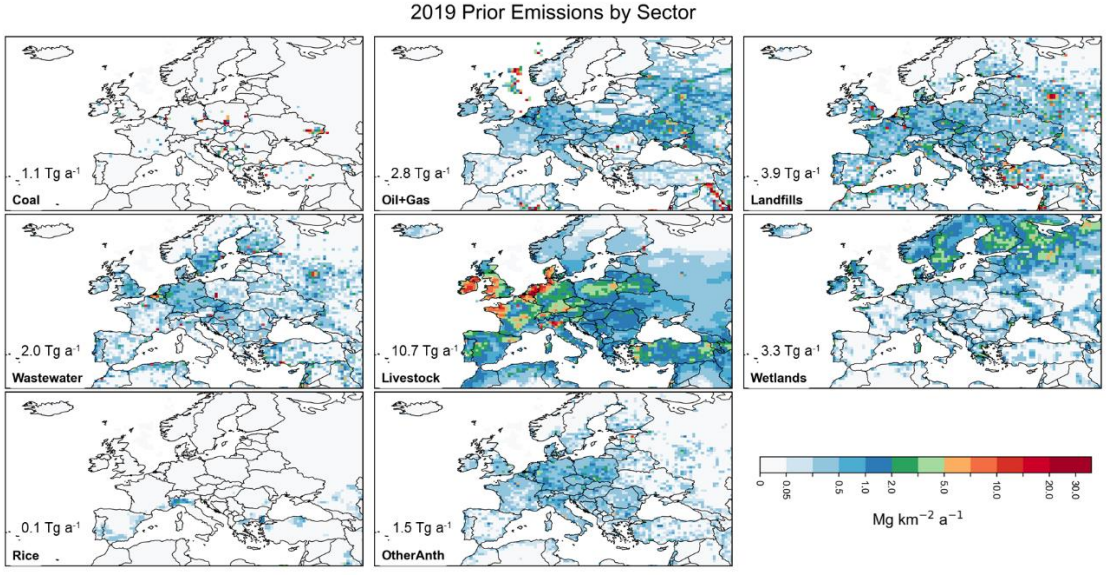

Figure 3: Spatial distributions of sectoral prior emissions for this inversion. Total sectoral emissions within the study domain are inset.

665

https://doi.org/10.5194/egusphere-2026-2165
Preprint. Discussion started: 10 June 2026

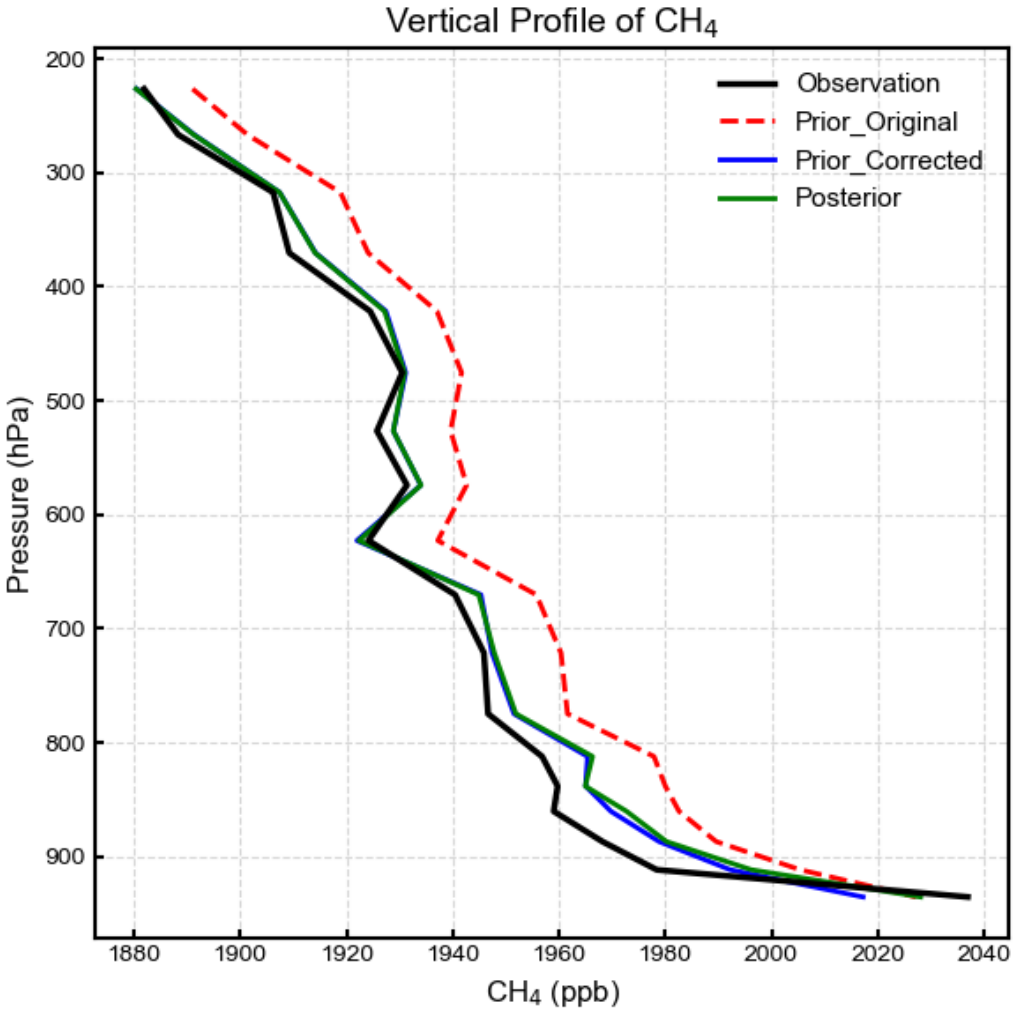

Figure 4: Comparison of simulated vertical profiles of methane mixing ratios with independent aircraft measurements from the IAGOS-CARIBIC project (https://www.caribic-atmospheric.com/Data.php). The black line represents average aircraft observations (Observation), the red line represents the prior simulation with unadjusted boundary conditions (Prior_Original), the blue line represents the prior simulation with bias-corrected boundary conditions (Prior_Corrected), and the green line represents the posterior simulation (Posterior). For this study, we selected methane measurements within the European region and confined to the troposphere, spanning from 2019 to March 2020, resulting in a total of 8,418 observations.

https://doi.org/10.5194/egusphere-2026-2165
Preprint. Discussion started: 10 June 2026

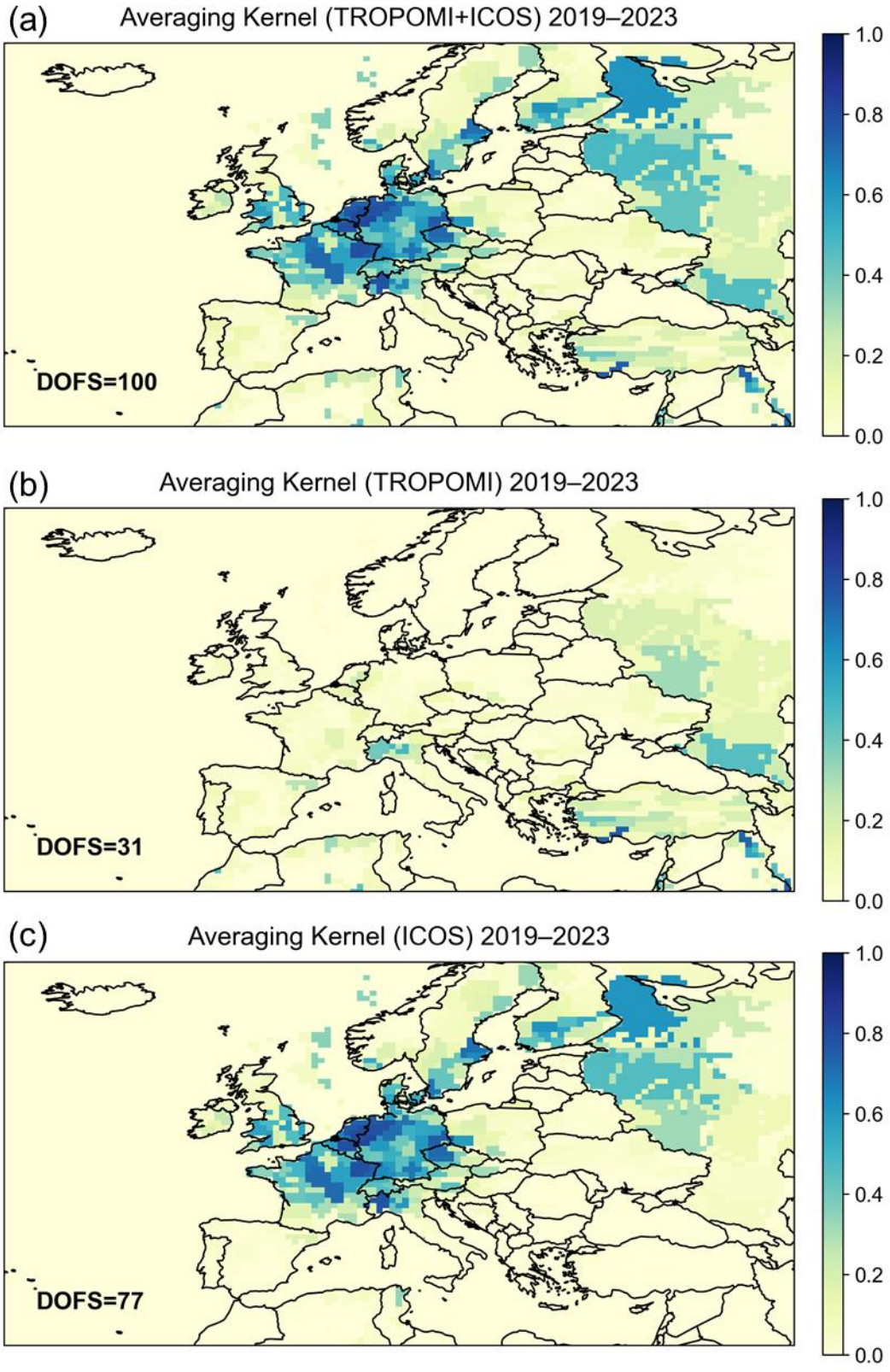

https://doi.org/10.5194/egusphere-2026-2165
Preprint. Discussion started: 10 June 2026

Figure 5: Spatial distribution of averaging kernel sensitivities for annual inversions of (a) satellite and surface (TROPOMI+ICOS) observations, (b) only satellite (TROPOMI) observations, and (c) only surface (ICOS) observations. DOFSs of these inversions for the entire domain are inset.

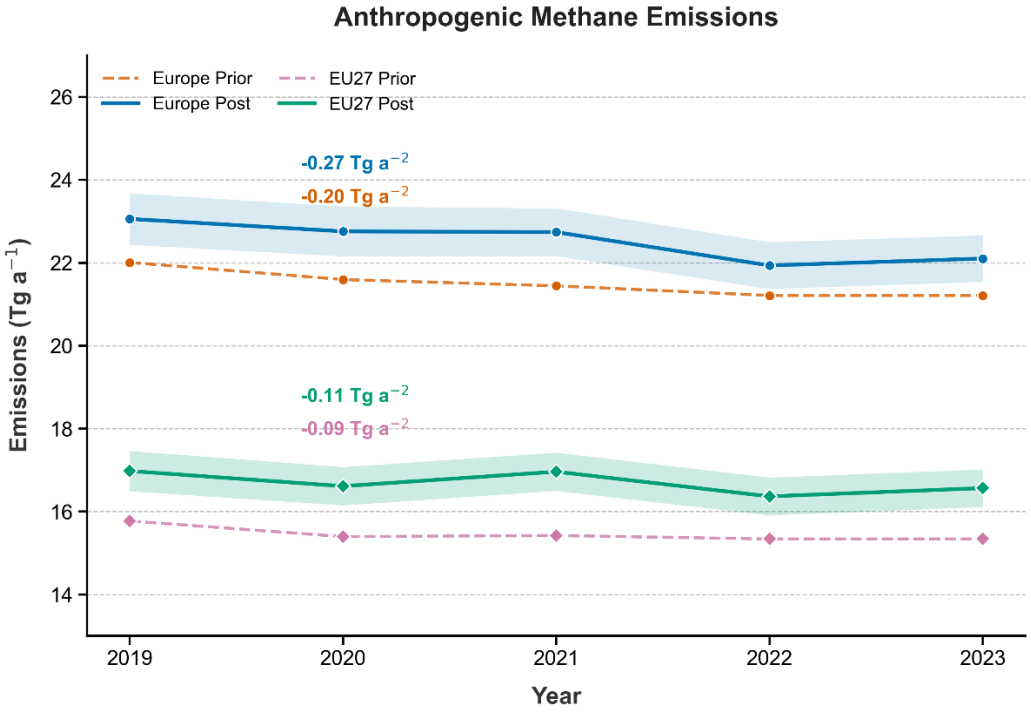

Figure 6: Time series of prior and posterior anthropogenic methane emissions from Europe and EU27. Color shadings represent the one standard deviation uncertainties of posterior estimates. Values of linear trends are inset.

https://doi.org/10.5194/egusphere-2026-2165
Preprint. Discussion started: 10 June 2026

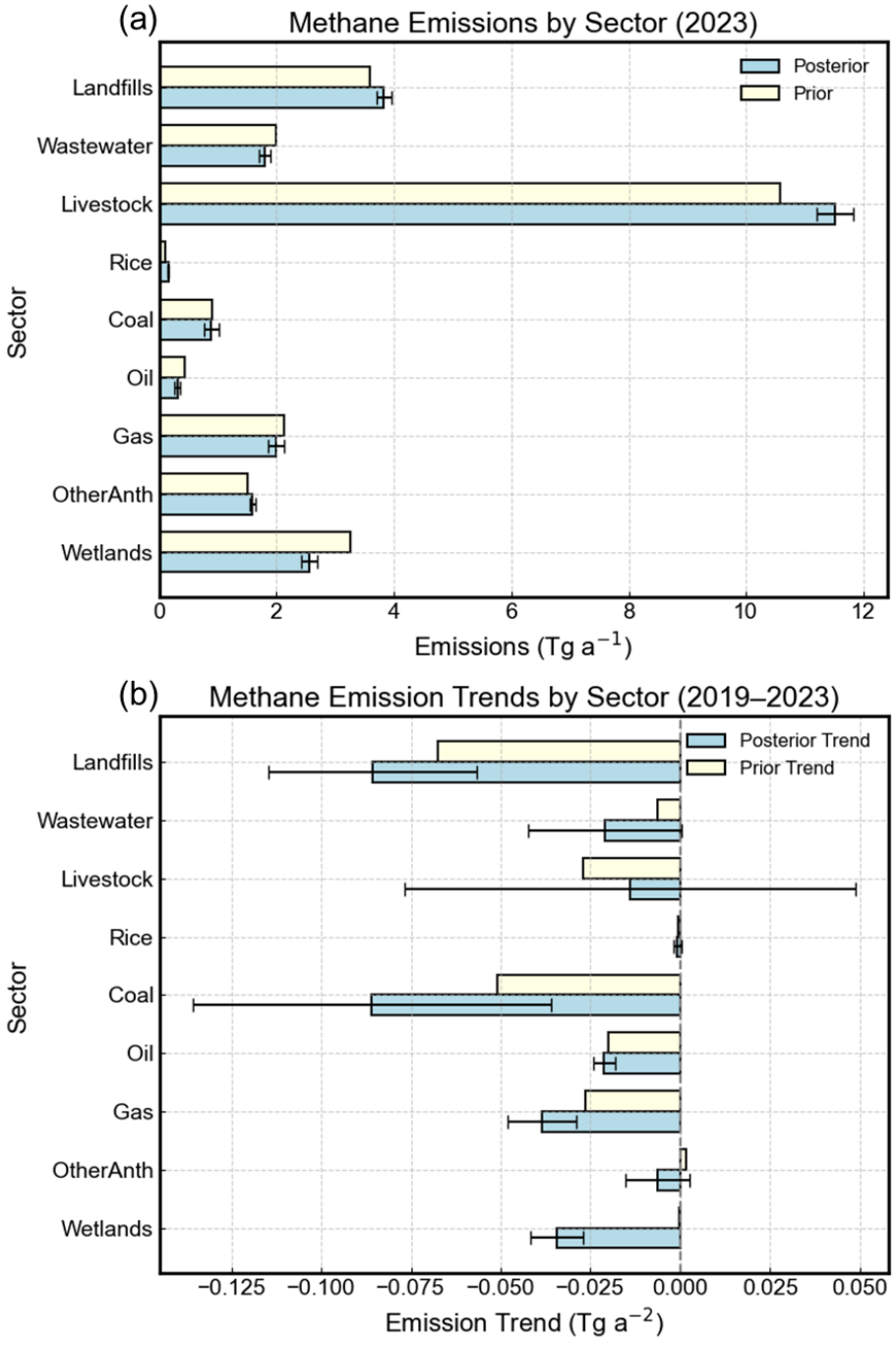

https://doi.org/10.5194/egusphere-2026-2165
Preprint. Discussion started: 10 June 2026

Figure 7: Europe's 2019–2023 average anthropogenic methane emissions (a) and their trends (b) by sector. Yellow bars represent prior estimates and blue bars posterior estimates. Error bars denote 1 standard deviation uncertainties of posterior estimates.

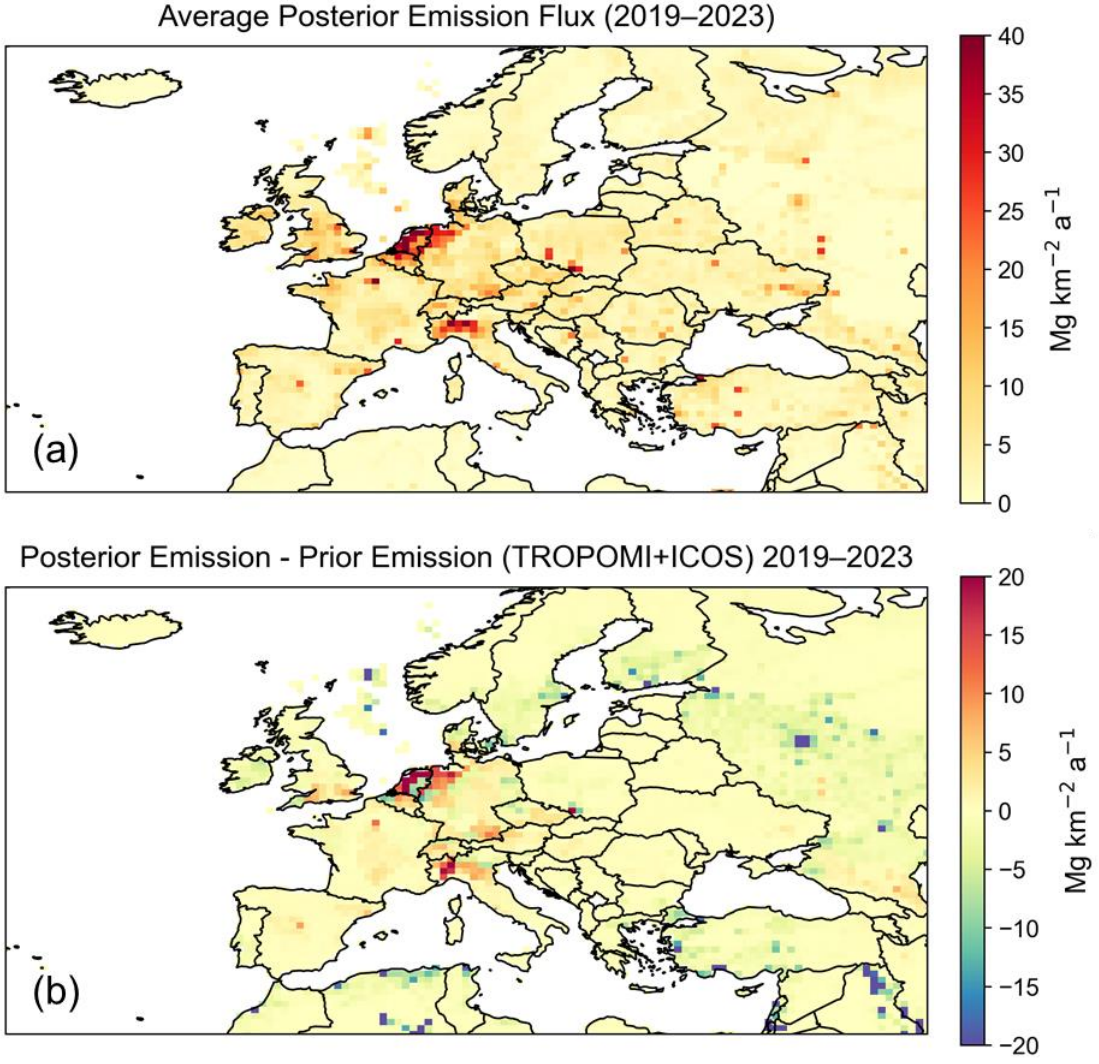

https://doi.org/10.5194/egusphere-2026-2165
Preprint. Discussion started: 10 June 2026

Figure 8: Spatial distributions of 2019–2023 average posterior methane emissions in Europe. (a) Five-year average posterior emissions; (b) Correction of methane emissions by the inversion expressed as posterior minus prior.

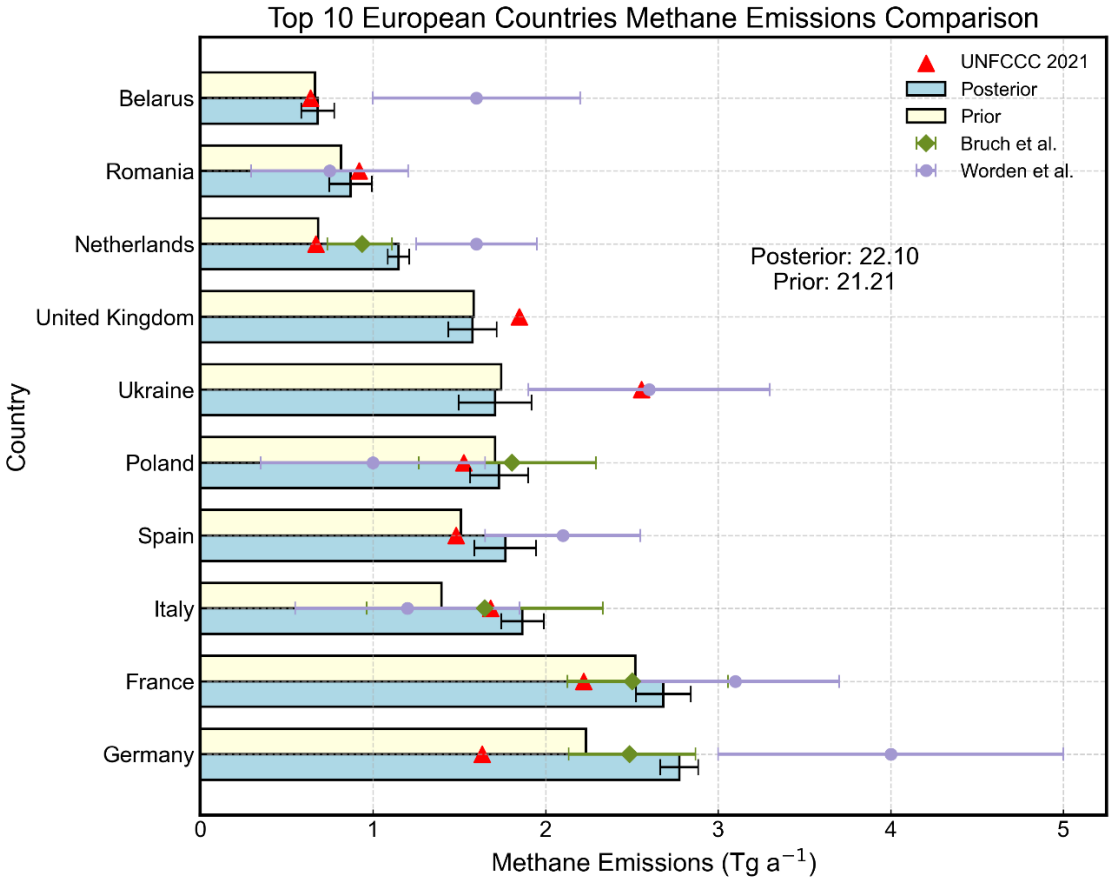

Figure 9: 2019–2023 anthropogenic methane emissions for top ten countries in Europe. Yellow bars represent prior emissions and blue bars posterior emissions. Results are compared with official reports to the UNFCCC (red triangles), a regional inversion of ICOS observations by Bruch et al. (2025) (green diamonds), and a global inversion of GOSAT satellite observation by Worden et al. (2022) for 2019 (purple circles). Error bars denote 1 standard deviation uncertainties of posterior estimates.

https://doi.org/10.5194/egusphere-2026-2165
Preprint. Discussion started: 10 June 2026

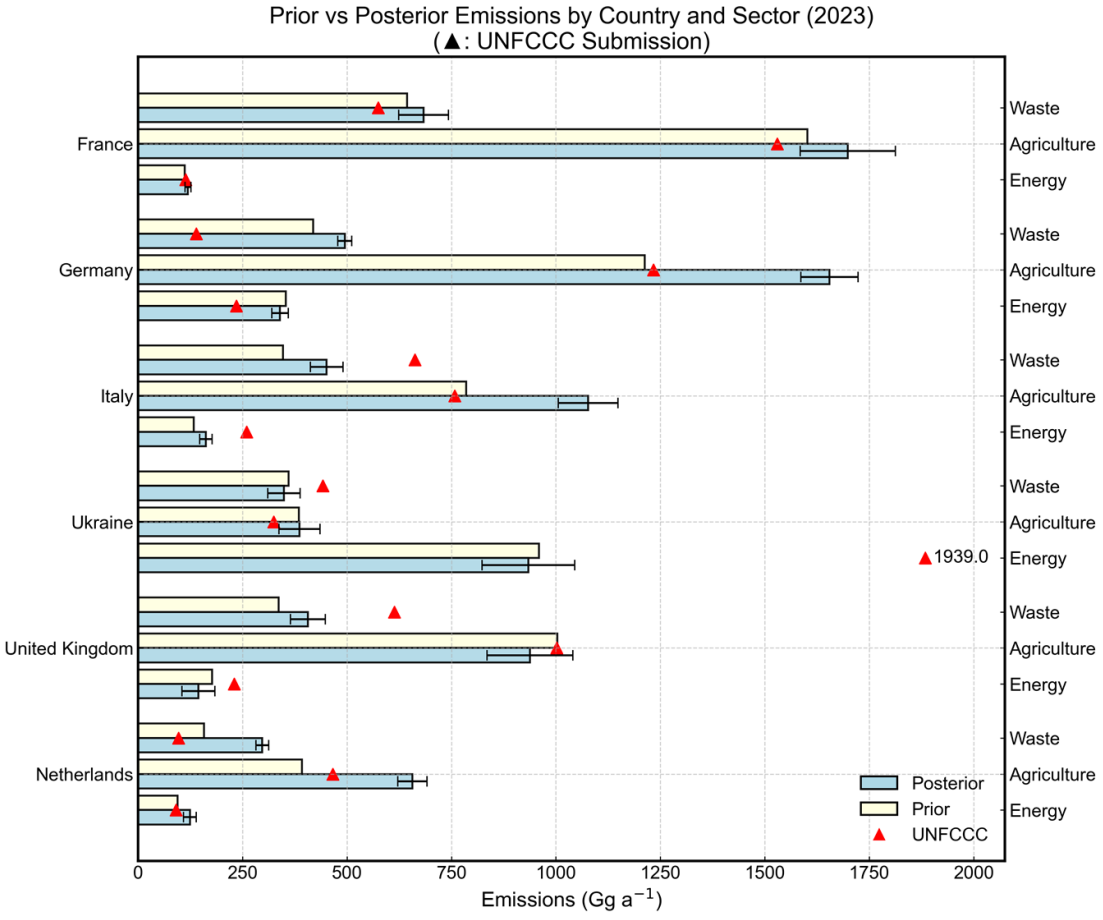

Figure 10: Sector breakdown of national anthropogenic emissions for six key countries in Europe. Yellow bars represent prior emissions, blue bars posterior emissions, and red triangles official reports to the UNFCCC as a comparison. Error bars denote 1 standard deviation uncertainties of posterior estimates. Based on the UNFCCC sectors, we group oil, gas, and coal as Energy, livestock and rice as Agriculture, and landfills and wastewater as Waste. IPPU and LULUC sectors, reported in UNFCCC data, are ignored, as their contributions are minor compared to agriculture, waste, and energy sectors (Figure 3).

https://doi.org/10.5194/egusphere-2026-2165
Preprint. Discussion started: 10 June 2026

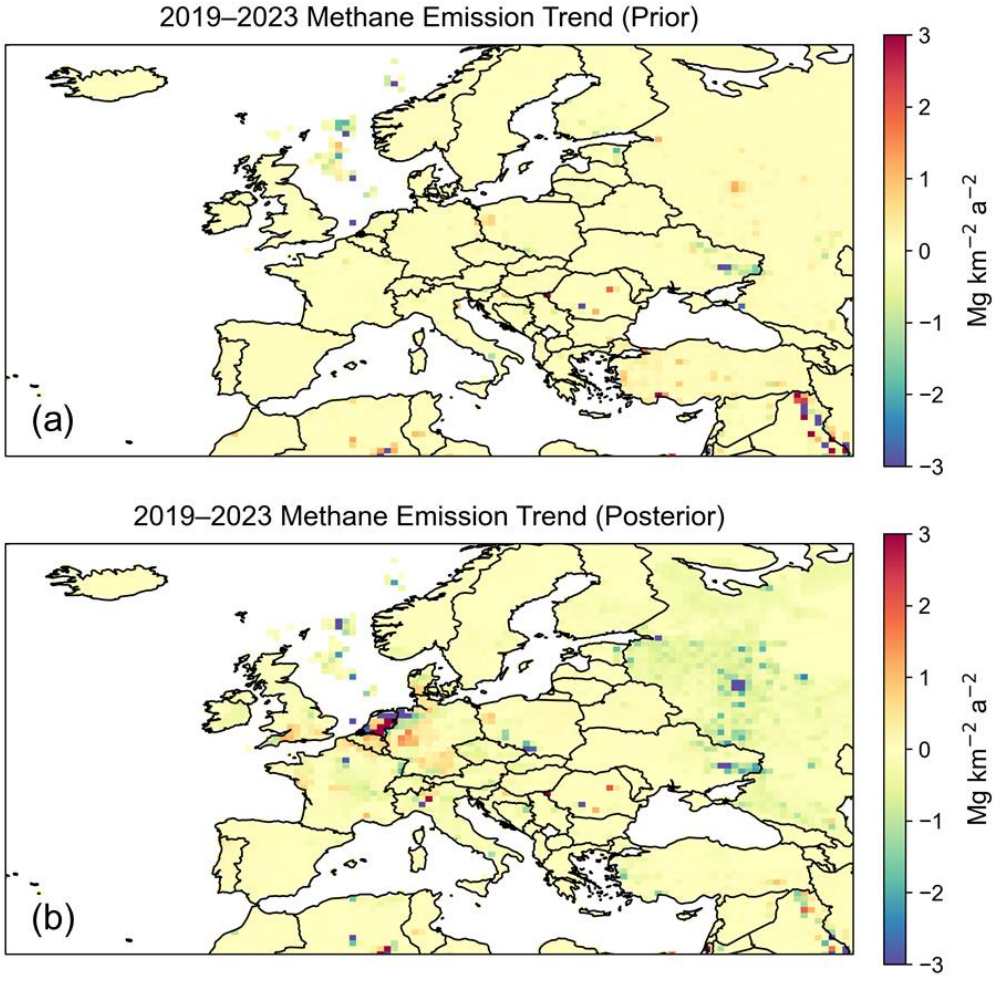

Figure 11: Spatial distributions of methane emission trends in Europe from 2019–2023. Linear trends in (a) prior and (b) posterior methane emissions.

https://doi.org/10.5194/egusphere-2026-2165
Preprint. Discussion started: 10 June 2026

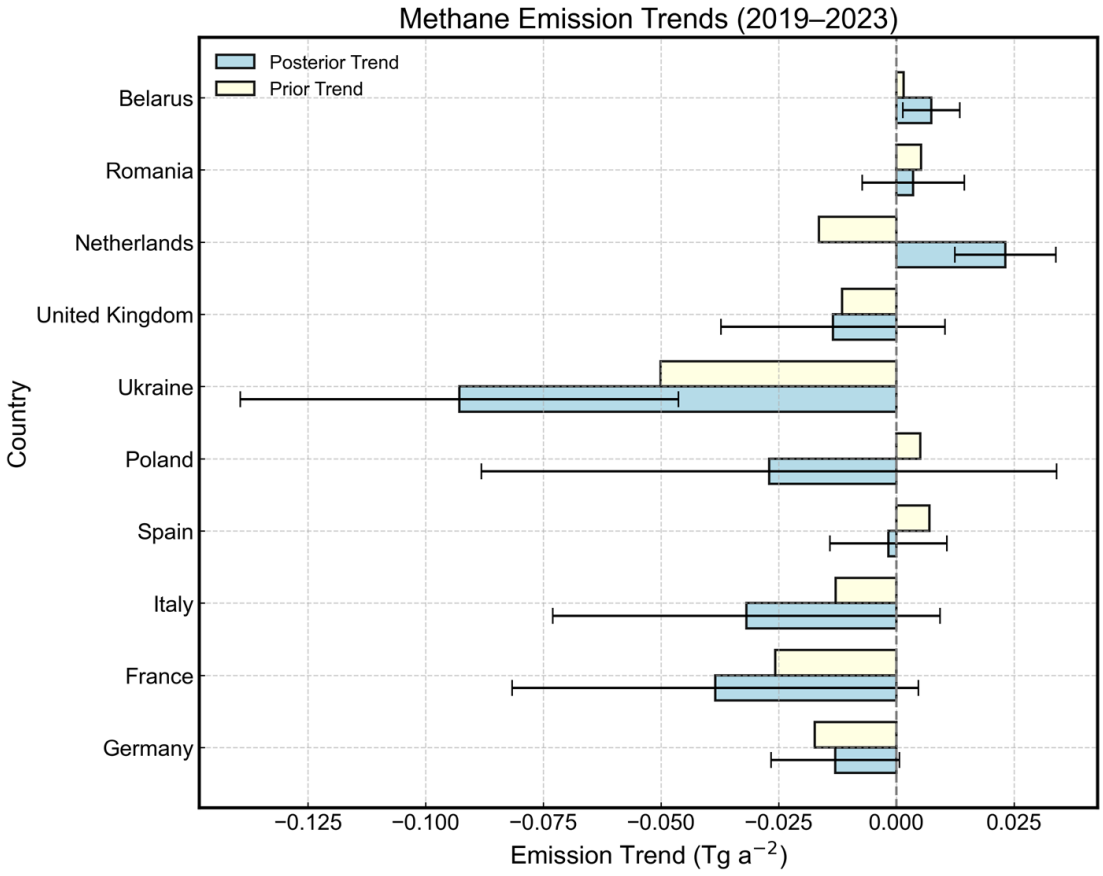

Figure 12: 2019–2023 trends in anthropogenic methane emissions for top ten countries in Europe. Yellow bars represent prior emissions and blue bars posterior emissions. Error bars denote 1 standard deviation uncertainties of posterior emission trends.